nature communications

Article

https://doi.org/10.1038/s41467-025-62976-4

# H2A.Z primes an epigenetic landscape for memory CD8$^+$ T cell recall response

Received: 11 November 2024

Accepted: 5 August 2025

Published online: 15 August 2025

Check for updates

Wei Liang[1,2], Jiyu Ding[3,4], Qian Chai[2], Mengjie Lv[2], Shuting Zheng[3,4], Xiangxiang Cao[3,4], Zhimin Wang[3], Xiaoling Ying[1], Wenqi Wu[1], Guohong Li[3] & Mingzhao Zhu[2,3,4]

The rapid recall ability is a hallmark of memory CD8$^+$ T cells, but the underlying mechanisms remain incompletely understood. Here we find that histone variant H2A.Z is expressed at higher levels in memory CD8$^+$ T cells than in naïve cells. Furthermore, in memory CD8$^+$ T cells H2A.Z is deposited at the promoters and enhancers, particularly super enhancers, of those genes involved in recall responses, while H2A.Z deficiency in memory CD8$^+$ T cells inhibits recall responses in vitro and in vivo. Mechanistically, multi-omics analyses show that H2A.Z maintains a poised epigenetic landscape on those recall response genes to potentiate a rapid transcription activation. Accordingly, H2A.Z deposition on these genes is induced by TCR/CD28 signals, and is cooperated by IL-7/IL-15 signals. Together, our data suggest that H2A.Z may orchestrate a specific epigenetic landscape during memory T cell differentiation to facilitate a rapid recall response.

Memory CD8$^+$ T cells are crucial for defending the body against acute and chronic infections, as well as cancers[1–3]. Inducing functional memory CD8$^+$ T cells is also essential for effective vaccine immunity[4,5]. These poised cells persist long-term and rapidly respond upon antigen re-exposure[6]. Compared to naïve T cells, memory T cells exhibit faster, more robust activation and effector function. This unique capacity enables efficient control of recurrent pathogens and cancers. A key question is how the rapid recall ability of memory T cells is established and regulated.

The molecular basis of the rapid recall response in memory T cells remains poorly understood. Early studies revealed differences at the protein level, particularly within T cell activation signaling pathways. While initial CD3 signaling events, as measured by CD3 complex and ZAP70 phosphorylation, are indistinguishable between memory and naïve CD8$^+$ T cells[7], memory CD8$^+$ T cells exhibit increased phosphorylation of LAT and ERK upon antigen stimulation. Another study reported quicker and enhanced nuclear translocation of NF-κB p50 in memory CD4$^+$ T cells compared to naïve cells following TCR stimulation[8]. Critically, however, these protein-level changes are transient modifications; they are not inherently stable and cannot be inherited through cell divisions during memory T cell homeostasis.

Epigenetic modifications represent heritable changes in chromatin states without altering the DNA sequence. Such modifications frequently accompany T cell activation and differentiation[9]. Recent studies implicate epigenetic programming as critical for the rapid recall response of memory T cells[10]. A genome-wide analysis of H3K4me3 and H3K27me3 in memory versus naïve CD8$^+$ T cells revealed significantly higher H3K4me3 deposition at poised gene loci in memory cells[11]. Bivalent chromatin domains, marked by both H3K4me3 and H3K27me3, were also enriched at silent gene loci in resting memory CD8$^+$ T cells; these genes were rapidly induced upon activation. Similarly, resting memory CD4$^+$ T cells exhibit an activating chromatin state at rapidly inducible genes (e.g., *IFNG*, *IL4* and *IL13*) associated with recall responses[12]. However, the mechanisms establishing this poised epigenetic landscape remain unclear.

H2A.Z, a highly conserved histone H2A variant, is incorporated into chromatin by ATP-dependent remodeling complexes in a replication-independent manner, influencing chromatin architecture

[1]Department of Urology, The Second Affiliated Hospital, Guangzhou Medical University, Guangzhou, China. [2]CAS Key Laboratory of Pathogenic Microbiology and Immunology, Institute of Microbiology, Chinese Academy of Sciences, Beijing, China. [3]Key Laboratory of Epigenetic Regulation and Intervention, Institute of Biophysics, Chinese Academy of Sciences, Beijing, China. [4]College of Life Sciences, University of Chinese Academy of Sciences, Beijing, China.
e-mail: zhumz@im.ac.cn

and gene regulation[13,14]. Recent studies demonstrate that H2A.Z deposition in gene promoter regions regulates nucleosome stability and increases chromatin accessibility. By weakening histone-histone interactions within the nucleosome[14–16], H2A.Z establishes a chromatin environment permissive for transcription factor and RNA polymerase II recruitment[17,18], enhancer RNA transcription, enhancer-promoter interactions[19], and ultimately modulates transcriptional activity. Additionally, H2A.Z influences histone modifications by recruiting complexes like MLL and PRC2 to promoters and enhancers, thereby regulating H3K4me3 and H3K27me3 methylation[18,20]. While extensively studied in yeast, plants, ESCs, and other model systems[14,21,22], the role of H2A.Z in T cells remains largely unexplored. Notably, in memory CD4$^+$ T cells, H2A.Z deposition occurs at *IFNG*, *IL4*, and *IL13* gene loci, correlating positively with other active chromatin marks[12]. A key outstanding question, therefore, is how H2A.Z contributes to the rapid recall response in memory T cells.

Here, transcriptome analysis reveals elevated expression of H2A.Z in memory CD8$^+$ T cells compared to naïve cells. Further investigation shows that H2A.Z is selectively enriched at the promoter and enhancer regions of key effector genes in resting memory T cells, establishing a poised chromatin state conducive to rapid transcriptional activation. This deposition is cooperatively regulated by TCR/CD28 and cytokine (IL-7/IL-15) signaling. Collectively, these findings uncover an H2A.Z-mediated epigenetic licensing mechanism in memory CD8$^+$ T cells that enables their rapid recall response. Targeting this epigenetic pathway may enhance the efficacy of vaccines and T cell-based immunotherapies.

## Results

### Identification of activation-recalled genes in memory CD8$^+$ T cells

Upon re-stimulation ex vivo, memory CD8$^+$ T cells rapidly activate their cytotoxic machinery[23]. To validate this rapid recall response in our study, the classical *Listeria monocytogenes*-OVA (LM-OVA) infection-induced OT-I memory T cell model was adapted[24]. Memory OT-I cells were identified and isolated from the LM-OVA infected mice at least 30 days later, as described previously[24]. Naïve OT-I cells were isolated from naïve OT-I transgenic mice. Equal number of memory and naïve OT-I cells were mixed and adoptively transferred (ATF) into recipient mice followed by LM-OVA rechallenge (Fig. 1a). The expansion of memory OT-I T cells is significantly higher than naïve OT-I T cells at day 4 or day 7 post-infection (Fig. 1b, c). To directly test the TCR signal per se on memory T cell recall and avoid the influence of other potential signals in vivo, resting memory and naïve OT-I T cells were isolated (Fig. 1d and Supplementary Fig. 1a, b) and stimulated with $OVA_{257\text{-}264}$ peptide in vitro. Significantly higher amount of IFN-γ was produced in memory OT-I T cells compared to naïve OT-I T cells (Fig. 1e). To more systemically evaluate the recall response of memory OT-I T cells, naïve and memory OT-I T cells were sorted and stimulated with anti-CD3 and anti-CD28 antibodies (Abs) for 6 or 24 hours (h), or left unstimulated for RNA-seq analysis (Fig. 1f and Supplementary Fig.1a, b). Principal-component analysis showed that stimulation caused potent transcriptomic change from the resting state in both memory and naïve OT-I cells (Fig. 1g). To characterize memory T cell recall response, we captured the genes that responded more robustly (at least 2-fold) at either 6 or 24 h in memory OT-I cells than in naïve OT-I cells, and defined these genes as memory T cell activation-recalled genes (ARGs). 80 ARG genes were up-regulated in memory OT-I cells compared to naïve OT-I cells (Supplementary Table 1). GO/KEGG analysis showed that these ARGs were enriched in functions such as "cytokine-cytokine receptor interaction", "regulation of MAPK cascade", "inflammatory response" (*Ifng*, *Ccl3* and *Xcl1*) and "immune effector process" (*Gzmb* and *Tnf*) (Fig. 1h, i). It is worth noting that memory T (IL-7R$^{high}$ KLRG1$^{low}$) cells include both central memory T ($T_{CM}$) and effector memory T ($T_{EM}$) cell populations (Supplementary Fig. 1c). To examine whether $T_{CM}$ and $T_{EM}$ may have different recall response, we isolate $T_{CM}$ and $T_{EM}$ separately and examine their recall response of the ARGs we previously defined using total memory T cells. The data show that both $T_{CM}$ and $T_{EM}$ have largely similar changes on these ARG induction compared to naïve cells (Supplementary Fig. 1d–f), suggesting a common phenotype of both $T_{CM}$ and $T_{EM}$ on the recall activation. Thus, these results validated the rapid recall response of memory CD8$^+$ T cells and defined a group of signature genes characterizing the recall response.

### H2A.Z regulates memory CD8$^+$ T cell recall response

To explore the epigenetic mechanism of memory T cell recall response, we selectively compared the expression of epigenetics-related genes between resting naïve OT-I T cells and LM-OVA infection-induced resting memory OT-I T cells. We plotted the log2 ratio of gene abundance between these two types of cells, and ranked all genes in the data set by increasing fold-change. It was observed that *H2afz*, encoding histone variant H2A.Z.1, is one of the top ranked genes highly expressed in resting memory OT-I cells (Fig. 2a), while *H2afv* (encoding histone variant H2A.Z.2) is not. Similar results were found using data from a previous study (Fig. 2b)[25]. Since H2A.Z.1 and H2A.Z.2 are highly conserved with only three amino acids difference, in the latter of this study we detected and manipulated total H2A.Z. At the protein level, significantly higher level of H2A.Z expression was found in memory OT-I T cells compared to naïve or effector OT-I T cells (Fig. 2c, Supplementary Fig. 2a), while no significant difference was found between naïve and effector cells (Supplementary Fig. 2a). Whether the increased expression of H2A.Z in memory T cells plays any important roles remains unknown. Recent studies have shown that H2A.Z is associated with "poised" genes[14]. We hypothesized that H2A.Z may regulate the recall response of "poised" memory T cells. To directly test this, we constructed a conditional knockout (cKO) mouse model, GzmB-Cre$^+$H2A.Z$^{f/f}$ OT-I mice (Supplementary Fig. 2b), in which H2A.Z is specifically deleted in CD8$^+$ T cells upon activation[26]. This model bypasses the potential influence of H2A.Z on T cell development and early effector response, therefore allowing us to study the role of H2A.Z in late effector response and memory formation. CD45.2$^+$ congenically marked naïve cKO OT-I or wild type (WT) OT-I cells were isolated and adoptively transferred separately into WT CD45.1 recipients, followed by LM-OVA infection. GzmB-Cre effectively deleted H2A.Z in effector OT-I T cells at day 7 (Supplementary Fig. 2c, d) and day 30 post-infection (Supplementary Fig. 2e). In addition, consistent with the purpose of this mouse model, GzmB-Cre-induced H2A.Z deletion does not affect OT-I T cell early activation and proliferation during the in vitro assay (Supplementary Fig. 3a–c). To explore whether H2A.Z influences naïve T cell primary response in vivo, CSFE-labeled naive WT and H2A.Z cKO OT-I T cells were transferred into WT mice, which were then infected with LM-OVA on the next day. At day 3 and 7 post-infection, the adoptively transferred OT-I T cells were analyzed. The results show that H2A.Z deficiency impairs OT-I cells proliferation (Supplementary Fig. 3d, e) and effector T cell survival (Supplementary Fig. 3f, g) in vivo.

To test whether H2A.Z influence memory T cell generation, WT and cKO naïve OT-I T cells were mixed transferred into WT host. Donor WT, donor cKO and host were congenically distinct. Mice were infected with LM-OVA and memory OT-I T cells were detected 30 days later. H2A.Z deficiency resulted in significantly reduced memory OT-I T cells (Supplementary Fig. 4a), but CD127 (IL-7R) expression was not significantly altered (Supplementary Fig. 4b, c), suggesting an important role of H2A.Z for memory T cell generation or maintenance. This is also consistent with our previous finding that H2A.Z is required for naïve T cell homeostasis proliferation[27]. To further elucidate the role of H2A.Z in memory T cell formation at early time, we employed an OT-I T cell co-transfer model and found that H2A.Z is required for OT-I MPEC differentiation at day 7 upon LM-OVA infection (Supplementary

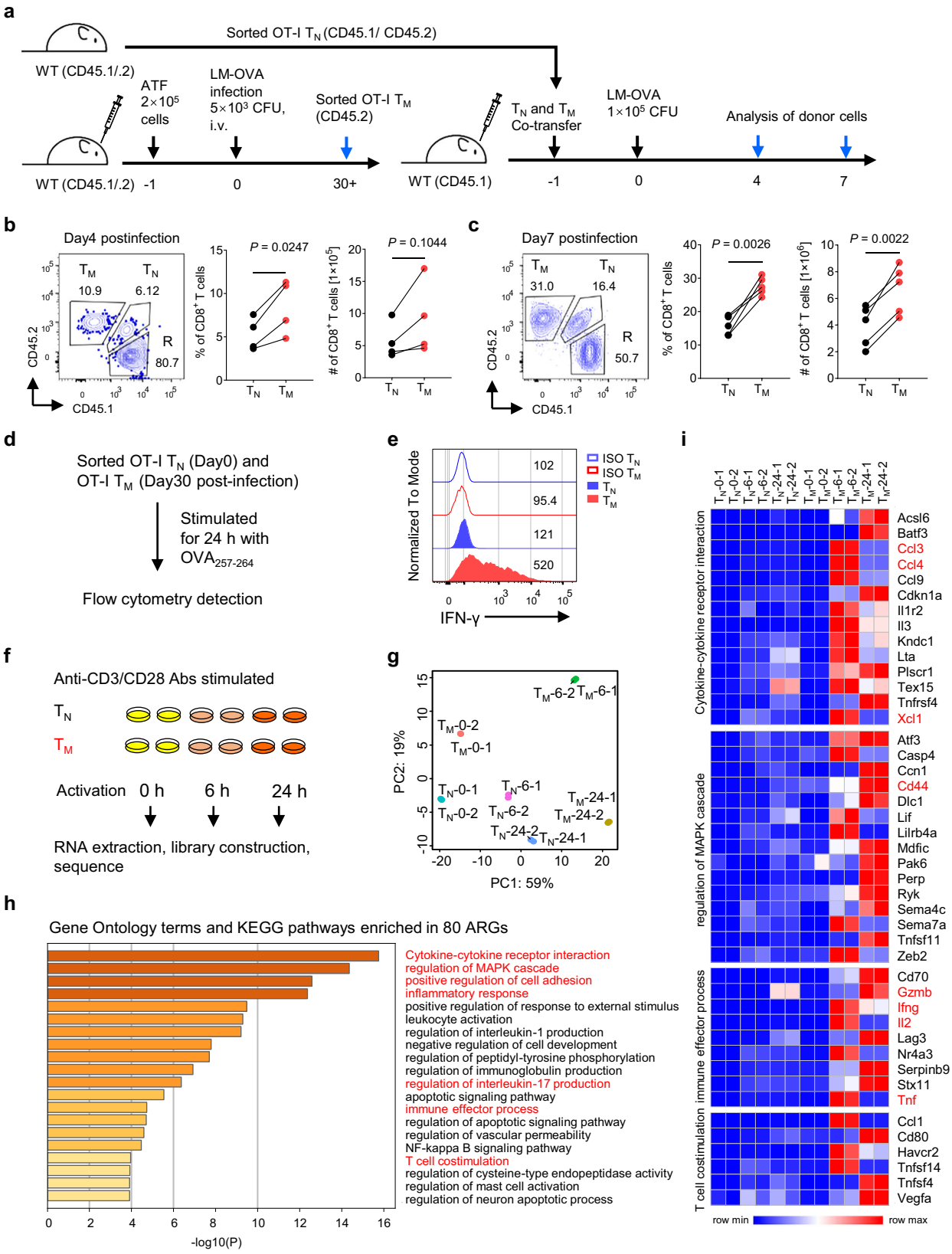


Fig. 4d, e) and the expression of CD127 is also reduced in H2A.Z deficient T cells (Supplementary Fig. 4f). To further investigate whether H2A.Z also regulates the maintenance of memory T cell, we have also analyzed the viability of memory T cells by flow cytometry at day 30 post-infection. The results showed that H2A.Z deletion did not affect the survival of memory T cells (Supplementary Fig. 4g). Thus, at least during the observed period, H2A.Z might play minor role for the maintenance of memory T cells. However, whether the long-term maintenance needs H2A.Z requires further study.

To specifically test the role of H2A.Z in memory T cell recall response, LM-OVA infection-induced memory OT-I T cells of WT and cKO genotypes were re-isolated and adoptively transferred with equal

**Fig. 1 | Memory CD8⁺ T cells respond rapidly and robustly than naïve CD8⁺ T cells. a** Experiment setup. CD45 congenically distinct naïve ($CD62L^{hi}CD44^{lo}$) OT-I cells ($T_N$) and memory ($CD127^{hi}KLRG1^{lo}$) OT-I cells ($T_M$) were sorted from spleens, mixed at a 1:1 ratio, and subsequently co-transferred into recipients, followed by infection with LM-OVA. **b**, **c** The frequencies of donor cells in the spleen of recipient mice were determined at day 4 ($n = 4$ mice) (**b**) and day 7 ($n = 5$ mice) (**c**) post-infection. **d** Experiment setup. Naïve ($CD62L^{hi}CD44^{lo}$) OT-I cells and memory ($CD127^{hi}KLRG1^{lo}$) OT-I cells were isolated from spleens for in vitro stimulation. **e** Resting memory and naïve OT-I cells were stimulated with $OVA_{257-264}$ peptide, IFN-γ production was determined by flow cytometry ($n = 3$ biologically independent samples). Values denote geometric mean fluorescence intensity (gMFI). **f** RNA-seq were performed as described in the schematic diagram ($n = 2$ biologically independent samples). **g** Principal components analysis (PCA). **h** Metascape analysis showing the Gene Ontology terms and KEGG pathways enriched in the list of ARG genes. **i**, Heatmap of selected genes from ARGs. Data are representative of two (**b**, **c** and **e**–**i**) independent experiments. Data are mean ± SD and the *P* value of two-tailed paired Student's t test (**b** and **c**). ATF, adoptively transferred. Source data are provided as a Source Data file.

number into a new set of recipient mice, followed by LM-OVA rechallenge (Fig. 2d). At day 7, significantly impaired recall response was found in cKO OT-I memory T cells compared to that in WT OT-I memory T cells (Fig. 2e).

To further specify the role of H2A.Z in memory T cells, a tamoxifen-induced gene deletion model, Rosa26-creERT2, was used[28]. H2A.Z deletion was induced in Rosa26-creERT2⁺$H2A.Z^{f/f}$ (icKO) OT-I T cells when memory has been fully established (day 45 after primary infection) (Supplementary Fig. 5a, b). H2A.Z icKO and WT OT-I memory cells were then isolated and mixed transferred to congenically distinct host. Their memory recall responses were detected upon LM-OVA rechallenge. Not only is recall expansion impaired in H2A.Z icKO OT-I cells (Fig. 2f–h), but the production of effector molecules such as IFN-γ and TNF-α (Fig. 2i, j and Supplementary Fig. 5c), as well as Perforin and Granzyme B (Supplementary Fig. 5d, e), is also significantly reduced. Together, these data suggest that H2A.Z regulates the recall response of memory CD8⁺ T cells in a cell-intrinsic mechanism.

To further examine the role of H2A.Z in human memory T cells, we knocked down its expression using the ProteanFect CRISPRMax-Cas9 mRNA Gene Editing Kit in an IL-7/IL-15-induced human CD8⁺ T cell memory in vitro system[29]. We then assessed the expression of the effector molecule IFN-γ following stimulation with either Human CD3/CD28 T Cell Activator or PMA/Ionomycin. The results showed that H2A.Z deficiency led to a reduction in IFN-γ expression in human CD8⁺ T memory cells upon re-stimulation. These results indicate that H2A.Z indeed plays a crucial role in the recall response of human memory CD8⁺ T cells (Supplementary Fig. 6a–d).

## Epigenetic features predetermine memory CD8⁺ T cell gene induction

To further define the molecular mechanisms underlying the rapid recall response in resting memory CD8⁺ T cells compared to naïve cells, we first profiled the global epigenome (including H2A.Z deposition, chromatin accessibility, H3K4me3, H3K27me3, H3K27ac and Pol II S5P enrichment) in memory and naïve OT-I T cells via native ChIP-seq, CUT&Tag, and ATAC-seq. Differential peak analysis revealed that H2A.Z is deposited differently in memory and naïve OT-I cells genome-wide (Supplementary Fig. 7a). Great Gene Regional Enrichment of Annotations Tool (GREAT)[30,31] analysis of the differential peaks showed distinct biological processes enriched in the two cell types (Supplementary Fig. 7a). The H2A.Z peaks specific to memory T cells were enriched with genes involved in "regulation of cell adhesion and activation" and "regulation of lymphocyte proliferation", etc., while naïve T cell-specific H2A.Z peaks are enriched with genes involved in "DNA damage checkpoint", "negative regulation of cell cycle process", "mitotic G1/S transition checkpoint", etc. These data suggest H2A.Z may mainly regulate activation in memory T cells while homeostasis in naïve T cells. Further analysis showed largely similar patterns of ATAC signal, H3K27ac and Pol II S5P between memory and naïve T cells (Supplementary Fig. 7b–d). However, H3K4me3 showed different patterns (Supplementary Fig. 7e). Memory T cell-specific H3K4me3 peaks are enriched with genes involved in "lymphocyte migration", "regulation of lymphocyte chemotaxis" and "protein acetylation", etc., while naïve T cell-specific H3K4me3 peaks are enriched with genes involved in "leukocyte cell-cell adhesion" and "T cell activation and differentiation", etc, probably suggesting H2A.Z-independent regulations. To further explore the global functions of H2A.Z in chromatin landscapes, we analyzed the chromatin accessibility and histone mark changes at the differential H2A.Z sites in naïve and memory T cells. The results showed that the permissive chromatin landscapes (such as chromatin accessibility and H3K4me3, H3K27ac and Pol II S5P) were highly enriched at the naïve T cell-unique H2A.Z sites in naïve T cells, but not in memory T cells (Supplementary Fig. 7f). In contrast, at memory T cell-unique H2A.Z sites, the permissive chromatin landscapes were also highly enriched in memory T cells, but not in naïve T cells (Supplementary Fig. 7f). These data suggested that highly enriched H2A.Z is associated with the deposition of permissive chromatin landscapes.

Induction of ARGs is characteristic of memory T cell recall response. Comparing the epigenetic features of ARG loci, we found memory T cells showed significantly higher deposition of H2A.Z on the ARG promoter regions, as well as enhancer regions (Fig. 3a, b). Furthermore, we also found that the ARG loci in resting memory OT-I T cells had other unique epigenetic features compared to those in resting naïve OT-I cells. These include lower levels of repressive H3K27me3 enrichment and higher levels of permissive H3K4me3, H3K27ac and Pol II S5P enrichment in the promoter and enhancer regions (Fig. 3a, b). These characteristic epigenetic features were typically observed in several important ARG gene loci (e.g., *Ifng*, *Gzmb*, *Ccl3*, *Ccl4* and *Xcl1*) (Fig. 3c). In contrast to the highly inducible ARGs, the silent genes, as defined in a previous study[12], showed significantly lower level of H2A.Z deposition, as well as deposition of H3K4me3, H3K27ac and Pol II S5P (Supplementary Fig. 8). Thus, the overall permissive epigenetic modifications may set ARGs at a poised state conferring rapid recall response of memory T cells.

The structure scheme of the super enhancer (SE) (Supplementary Fig. 9a) illustrates its key role in the gene transcription process. It recruits transcription factors and RNA polymerase II to target gene promoters and promotes the formation of the mediator co-activator complex[30]. H3K27ac is a commonly used hallmark to identify putative genome-wide enhancers[32]. Since we found that the enrichment of H3K27ac is significantly increased at ARG gene loci in memory OT-I T cells than in naïve OT-I cells (Fig. 3b), we hypothesized that SEs may exhibit differences in memory and naïve OT-I cells. To obtain a genome-wide landscape of SEs in memory T cells, we analyzed H3K27ac signal in memory and naïve OT-I T cells through the rank ordering of super-enhancers (ROSE) algorithm[30]. We identified 559 super-enhancer regions in memory T cells (Supplementary Fig. 9b), much more than in naïve OT-I cells (56 super-enhancer regions) (Supplementary Fig. 9c), indicating their significance in memory T cell function. Specifically, 9 of ARGs in memory OT-I cells (Supplementary Fig. 9d), including *Ifng*, *Gzmb*, *Ccl3*, *Ccl4* and *Xcl1*, are associated with super enhancers, while none was found associated with SE in naïve OT-I T cells (Supplementary Fig. 9e).

## H2A.Z establishes the poised epigenetic features of ARGs in memory T cells

To further investigate the relationship between H2A.Z deposition and the other epigenetic features, we profiled the epigenome in WT and H2A.Z cKO memory OT-I T cells. In WT memory OT-I cells, at the genome-wide, H2A.Z is consistently correlated with chromatin

https://doi.org/10.1038/s41467-025-62976-4

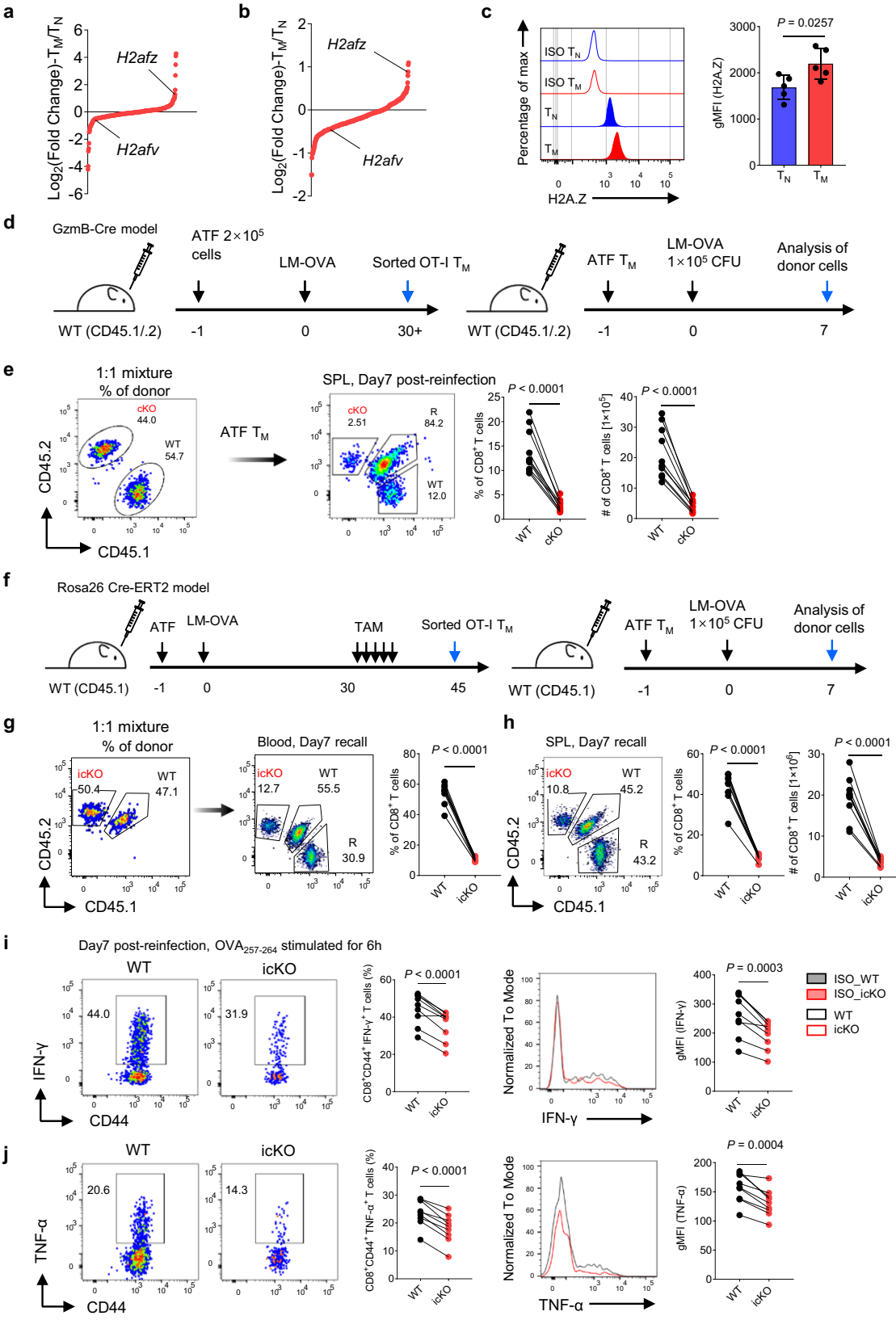


accessibility, as well as with marks of gene activation such as H3K4me3 and H3K27ac, but H2A.Z is poorly associated with the gene silencing mark H3K27me3 in the promoter and enhancer regions (Fig. 4a, b). To specifically determine the effect of H2A.Z on ARG loci, we compared WT and H2A.Z cKO memory OT-I T cells. The data demonstrate that H2A.Z depletion significantly alters the epigenetic landscape of ARG promoters and enhancers in resting memory T cells, including decreased chromatin accessibility, reduced levels of Pol II S5P and the active histone marker H3K27ac, and increased levels of the repressive histone marker H3K27me3 (Fig. 4c–e). Thus, H2A.Z may serve as "a master regulator" in memory $CD8^+$ T cells to establish a permissive poised epigenetic landscape on ARG loci for rapid recall response.

**Fig. 2 | Conditional deletion of H2A.Z reduces Ag-specific memory CD8⁺ T cell recall responses. a**, **b** The log2 ratio of gene abundance between the memory and naïve OT-I cells, line plot with genes ranked according to increasing log2 ratios. Based on data from Fig. 1F (**a**) and GEO dataset GSE15907 (**b**). **c** H2A.Z expression was analyzed in naïve ($CD62L^{hi}CD44^{lo}$) and memory ($CD127^{hi}KLRG1^{lo}$) OT-I cells ($n = 5$ mice per group). Values denote geometric mean fluorescence intensity (gMFI). **d** Experiment setup. CD45 congenically distinct naïve OT-I cells from wild-type (WT) and GzmB-Cre H2A.$Z^{f/f}$ (cKO) OT-I mice were mixed at a 1:1 ratio and co-transferred into recipients. On the next day, these mice were infected with LM-OVA. On day 30-45, WT and cKO memory OT-I cells were sorted and re-mixed at a 1:1 ratio ($1.5 \times 10^4$ mixed cells/mice) and co-transferred into congenically marked WT recipients and followed by LM-OVA infection. **e** At day 7 post-infection, the frequencies of donor cells in the spleen of recipient mice were determined ($n = 10$ mice). **f** Experiment setup. CD45 congenically distinct naïve OT-I cells from WT and Rosa26 cre-ERT2 H2A.$Z^{f/f}$ (icKO) OT-I mice were mixed at a 1:1 ratio and transferred into recipients. On the next day, these mice were infected with LM-OVA. After TAM injection, WT and icKO memory OT-I cells were sorted and re-transferred into congenically marked WT recipients and followed by LM-OVA infection. **g**, **h** On day 7 post-infection, the frequencies of donor cells in the blood (**g**) and spleen (**h**) of recipient mice were determined ($n = 10$ mice). **i**, **j** Splenocytes isolated from recipient mice were stimulated with the $OVA_{257-264}$ peptide for 6 h, then cytokine production from OT-I cells was measured. Values denote gMFI ($n = 9$ biologically independent samples). Data are representative of two independent experiments in (**c**), three independent experiments in (**e** and **g**–**j**). Data are mean ± SD. Statistical analysis was performed using two-tailed unpaired Student's t test (**c**) or two-tailed paired Student's t test (**e** and **g**–**j**). Source data are provided as a Source Data file.

Since we found that the enrichment of H3K27ac is significantly decreased at ARG gene loci in H2A.Z deficient memory OT-I T cells (Fig. 4e), we hypothesized that H2A.Z may also regulate SEs at ARG gene loci in memory T cells. Indeed, deficiency of H2A.Z in memory OT-I T cells results in a significant decrease in H3K27ac levels at SE regions at genome-wide (Supplementary Fig. 9f). Moreover, at the SE regions of ARGs, H3K27ac levels are also significantly decreased in H2A.Z deficient memory OT-I cells (Supplementary Fig. 9g), as specifically demonstrated in *Ifng, Gzmb, Ccl3, and Ccl4* loci (Supplementary Fig. 9h). Thus, H2A.Z might not only regulate ARG poised induction at regular promoter and typical enhancer regions in memory T cells, but also via SE.

### H2A.Z regulates ARG induction during memory T cell recall response

Our data showed that H2A.Z plays an important role in the establishment of poised epigenetic landscape in ARG loci. Whether it is required for ARG induction during memory T cell recall response is still unknown. To do this, LM-OVA infection-induced WT and cKO memory OT-I cells were isolated and stimulated in vitro with $OVA_{257-264}$ peptide (Fig. 5a). RNA-seq analysis was performed for transcriptome comparison. The results show that H2A.Z deficiency in memory OT-I cells significantly reduced the induction of genes related to "cytokine-cytokine receptor interaction", "chemotaxis" (*Ifng*, *Gzmb*, *Ccl3* and *Tnfsf11*) and "regulation of interleukin-17 production" (*Ccn1*, *Ccl1* and *Tnfsf14*) (Fig. 5b). Specifically, impaired ARG induction was also found by gene set enrichment analysis (GSEA) (Fig. 5c), including *Ifng, Gzmb, Tnf, Il2, Xcl1, Ccl3, Ccl4*, etc. (Fig. 5d). Some of them were also confirmed by qPCR (Fig. 5e). Flow cytometric analysis showed that cKO memory OT-I cell also produced reduced levels of IFN-γ and Granzyme B, upon $OVA_{257-264}$ peptide (Fig. 5f) or IL-12/IL-18 restimulation (Fig. 5g). Moreover, TAM-induced icKO memory OT-I cell showed consistent results, including reduced levels of IFN-γ, TNF-α and Granzyme B, upon $OVA_{257-264}$ peptide (Supplementary Fig. 10a–c) or IL-12/IL-18 restimulation (Supplementary Fig. 10d). These data provided direct evidence that H2A.Z is a master regulator to facilitate ARG induction in memory $CD8^+$ T cells for their recall response.

ARGs is a set of genes that are quickly/robustly induced upon re-stimulation in memory T cells. In addition to ARG, many other genes are also induced upon re-stimulation in memory T cells, although in a lower degree compared to ARGs. We determined them as activation induced genes (AIGs) hereafter for comparison. In the deficiency of H2A.Z, significant number of AIGs also showed impaired induction in memory T cells upon stimulation at genome-wide (Supplementary Fig. 11a), suggesting a general effect of H2A.Z for gene induction. Comparing the level of H2A.Z deposition, we found these AIGs are even deposited higher levels of H2A.Z at their promoters compared to those on ARGs (Supplementary Fig. 11b). These data revealed that H2A.Z deposition level is not positively correlated with the induction speed or extent of corresponding genes. Moreover, during secondary expansion, many other genes are induced at later time points, our data showed that many genes are also controlled by H2A.Z at Day7 post-reinfection (Supplementary Fig. 11c–e).

### TCR/CD28 and IL-7/IL-15 signals coordinately induce H2A.Z deposition at ARG loci

The preceding data indicates that H2A.Z regulates the expression of ARG via epigenetic priming. However, it is still unclear which signals drive the enrichment of H2A.Z at ARG gene loci. T cell activation signals (TCR/CD28 signaling) and cytokine signals (IL-7 or IL-15, etc.) are crucial signals controlling memory $CD8^+$ T cell formation[33,34]. We wondered that the deposition of H2A.Z in memory T cells might be regulated by these signals. To do this, naïve OT-I T cells were stimulated for a short-term with different extracellular signals (TCR/CD28, IL-7, IL-15) to evaluate their early and direct effect on H2A.Z deposition (Fig. 6a). PCA analysis of genome-wide differential peaks highlighted significant differences between the groups, which were largely driven by TCR signaling, as shown in PC1 (Fig. 6b). Differential peak analysis showed that TCR/CD28 and cytokine signals caused extensive and differential H2A.Z enrichment genome-wide in $CD8^+$ T cells (Fig. 6c). Gene Regional Enrichment of Annotations Tool (GREAT) analysis[35] on differential peaks showed distinct biological processes regulated by TCR/CD28 and IL-7 combination signals compared to TCR/CD28 signals alone (Fig. 6d), while TCR/CD28 and IL-15 combination signals are largely similar to TCR/CD28 signals alone, suggesting the differential role IL-7 and IL-15 on H2A.Z deposition selection. TCR/CD28 signals induced H2A.Z deposition on genes related to "regulation of adaptive immune response", "regulation of TNF, IFN-gamma, and IL-2 production", etc. TCR/CD28 and IL-7 combination signals induced H2A.Z deposition on genes related to "regulation of cell activation", "cytokine production", "cell adhesion and proliferation", and "chromatin organization and remodeling".

Next, we further analyzed whether TCR/CD28 and cytokine signals may promote the enrichment of H2A.Z at ARG loci. Interestingly, TCR/CD28 signals alone induced dramatically increased H2A.Z deposition at ARG gene loci, and additional IL-7 or IL-15 signal further but only slightly increased H2A.Z deposition (Fig. 6e). However, at specific gene level, the differential roles of these signals are more obvious. For instance, TCR/CD28 signals alone appear to be sufficient to induce H2A.Z deposition at effector gene loci (*Ifng* and *Gzmb*) (Fig. 6f), while cytokine signals contribute significantly to H2A.Z deposition on chemokine gene loci (*Ccl3*, *Ccl4* and *Xcl1*) (Fig. 6f). These data suggest that H2A.Z deposition is primarily regulated by TCR/CD28 signals, with specific gene loci also being influenced by cytokine signals cooperatively.

## Transcription factors mediate site-specific H2A.Z deposition and ARG induction

We then further wondered how TCR/CD28 signals could induce H2A.Z deposition on ARG loci. We specifically focused on *Ifng*, a key ARG for memory T cell recall response. MOTIF analysis of H2A.Z binding sites

https://doi.org/10.1038/s41467-025-62976-4

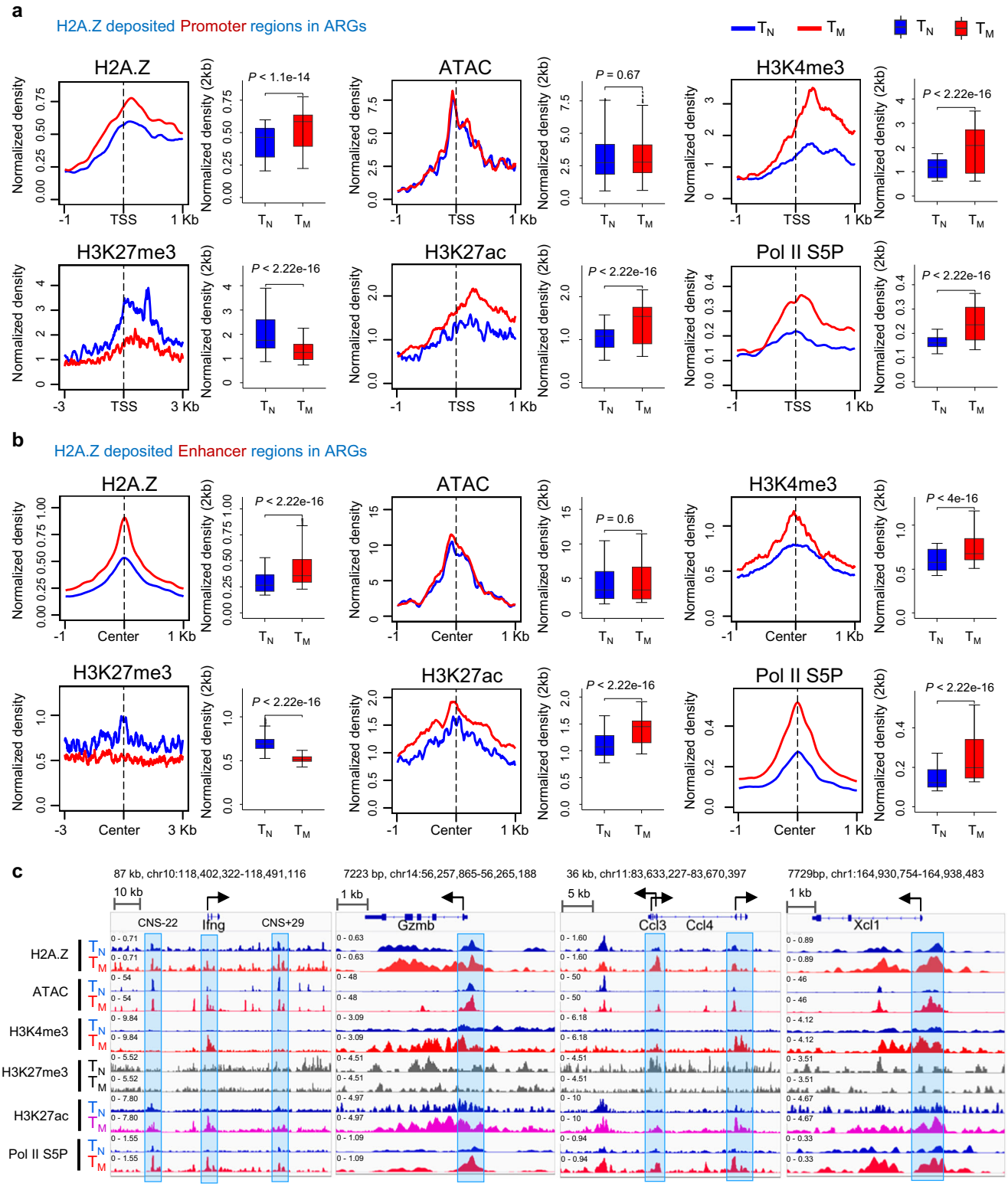


**Fig. 3 | Epigenetic features predetermine memory CD8⁺ T cell gene induction.** **a**–**c** Naïve (CD62L$^{hi}$CD44$^{lo}$) OT-I CD8$^{+}$ splenocytes and day 30-45 post-infection memory (CD127$^{hi}$KLRG1$^{lo}$) OT-I cells were sorted from spleens. H2A.Z and Pol II S5P CUT&Tag-seq were performed (n = 2 biologically independent samples per group). Data are representative of two independent experiments. Other data (ATAC-seq, H3K4me3, H3K27me3 and H3K27ac) in the Figure are from published data (GSE89036). The Figure shows the density of peaks around TSS (**a**) and enhancer regions (**b**). Box plots showing signal strength of inducible gene locus in $T_N$ and $T_M$ using normalized read counts of ATAC-seq and ChIP-seq or CUT&Tag-seq peaks in each condition. Statistical significance was determined with two-sided paired Wilcoxon test. **c** Sequencing tracks at selected gene loci as displayed on the Integrative Genomics Viewer (IGV), with gene structure and transcription orientation marked on the top. CNS, conserved non-coding sequence elements.

https://doi.org/10.1038/s41467-025-62976-4

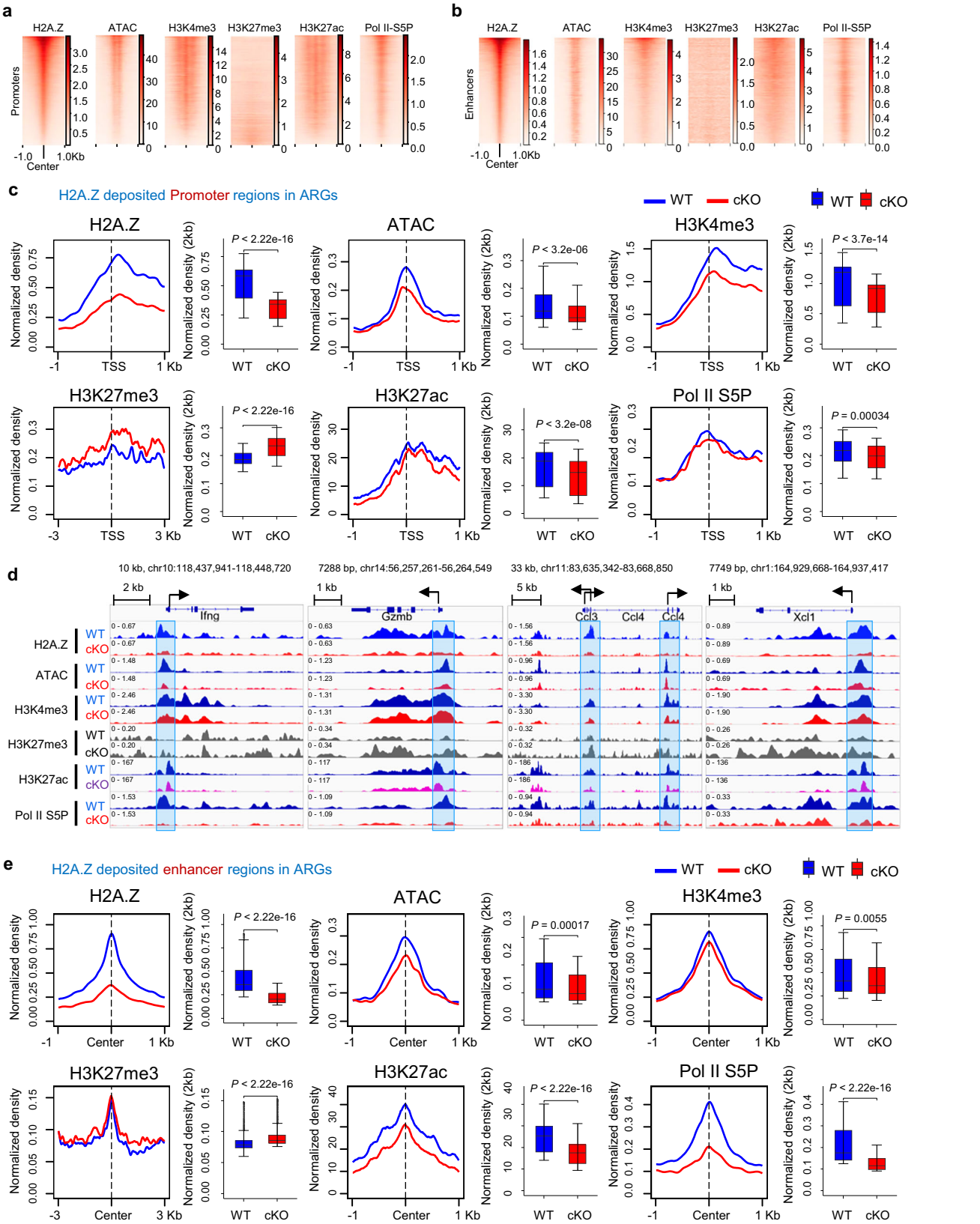


on *Ifng* promoter and enhancer regions showed many consensus binding motifs of several transcription factors (TF) of AP-1 family and RUNX family. AP-1 family is one of the major TFs downstream of TCR signaling[36]. We hypothesized that AP-1 might be involved in H2A.Z deposition on these sites. To avoid the redundancy of AP-1 family or even other TFs, we chose to delete the specific TF-binding motif by CRISPR-Cas9 technique in EL4 cells to test this hypothesis (Fig. 7a, Supplementary Fig. 12a). The targeting of the TF-binding motif successfully led to motif mutation manifested as single or multiple nucleotide deletions or additions within the motif as determined by DNA sequencing of targeted cells (Supplementary Fig. 12b–d). Disruption of AP-1 binding motif of 15 bp nucleotides at the promoter

**Fig. 4 | H2A.Z deletion leads to chromatin landscape changes in memory T cells.** **a**–**e** Naïve OT-I cells sorted from the spleens of WT (OT-I H2A.Z$^{f/f}$) or cKO (OT-I H2A.Z$^{f/f}$ GzmB-Cre) mice were transferred into hosts, followed by LM-OVA infection. Day 30-45 post-infection memory (CD127$^{hi}$KLRG1$^{lo}$) OT-I cells were sorted from spleens. ATAC-seq and CUT&Tag were performed ($n = 2$ biologically independent samples per group). Data are representative of two independent experiments. **a**, **b** Heat map comparing enrichment signals of H2A.Z, ATAC, H3K4me3, H3K27me3, H3K27ac and Pol II S5P at promoter regions (TSS) and enhancer regions in wild-type $T_M$ cells. All heatmaps were generated using the same ordered regions ranked by decreasing H2A.Z levels in $T_M$ cells. **c** The Figure shows the density of peaks around TSS. **d** Genome browser snapshots for representative genomic loci showing H2A.Z enrichment and various epigenetic marks. **e** The Figure shows the density of peaks around enhancer regions. Box plots showing signal strength of inducible gene locus in WT and cKO $T_M$ cells using normalized read counts of ATAC-seq and ChIP-seq or CUT&Tag-seq peaks in each condition. Statistical significance was determined with two-sided paired Wilcoxon test.

region (TSS) of *Ifng* caused a decrease in H2A.Z deposition in both resting and activated EL-4 cells (Fig. 7b). Additionally, disturbance of the overlapping JUN and RUNX family binding motif of 15 bp nucleotides at the enhancer region (conserved non-coding sequence elements 22, CNS-22) upstream of *Ifng* also resulted in reduced H2A.Z deposition in resting and activated EL-4 cells (Fig. 7c). Similarly, altering the RUNX family binding motif of 12 bp nucleotides at the enhancer region (CNS+45) downstream of *Ifng* also led to reduced H2A.Z deposition in resting and activated EL-4 cells (Fig. 7d). More importantly, the induction of *Ifng* gene expression during EL-4 activation was significantly diminished when these TF binding motifs were mutated (Fig. 7e–g).

To evaluate the role of specific TF binding motifs in primary CD8$^+$ T cells, we utilized a retrovirus-based CRISPR-Cas9 technique[37] to mutate these motifs in primary murine OT-I T cells (Fig. 7h). Non-targeted and targeted OT-I cells were then co-transferred at 1:1 ratio into congenically marked WT recipient mice, which were then infected by LM-OVA and memory OT-I cells were isolated at day 30 post-infection for in vitro re-stimulation to determine their recall response. IFN-γ was measured by flow cytometry. The results showed that mutations in the specific TF-binding motifs located at the TSS, CNS-22, or CNS+45 regions led to a significantly decreased expression of IFN-γ in primary CD8$^+$ T cells (Fig. 7i–k).

Together, these data suggest that the enrichment of H2A.Z at the gene loci of *Ifng* is regulated by specific TFs, and disruption of the TF binding motifs decreases the deposition levels of H2A.Z, ultimately leading to reduced induction of the target genes.

## Discussion

It is well-established that memory T cells mount faster and more robust responses than naïve T cells upon antigen stimulation. However, the molecular mechanisms underlying this rapid recall ability remain poorly defined. In this study, we demonstrate that genes enabling rapid recall (activation-recalled genes, ARGs) exhibit a distinct epigenetic landscape at their promoter and enhancer regions in memory T cells compared to naïve T cells. Notably, H2A.Z emerges as a key regulator of this poised epigenetic state. Genetic deletion of H2A.Z in primary T cells reversed activating epigenetic features to a repressive chromatin state (Fig. 8). Consequently, H2A.Z-deficient memory T cells exhibited impaired recall responses both in vitro and in vivo. These findings provide direct evidence that H2A.Z-dependent epigenetic mechanisms critically regulate the rapid recall response of memory T cells.

In this study, we generated foreign antigen (OVA)-specific memory OT-I T cells using the LM-OVA infection mouse model. This approach closely mimics memory T cells generated by natural infection or vaccination. This is different from the previous study in which spontaneously generated human virtual memory T cells were used[11]. In addition, total memory CD8$^+$ T cells were analyzed in our current study rather than separated subsets of central memory and effector memory CD8$^+$ T cells. We identified typical effector genes of the memory recall response as ARGs, defined by their capacity for faster or more robust functional responses in resting memory versus naïve T cells upon stimulation. These ARGs included cytotoxic molecules (*Gzmb*), cytokines (*Tnf*, *Il2*, *Ifng*, *Lta*), chemokines (*Ccl3*, *Ccl4*, *Xcl1*), costimulatory molecules (*Havcr2*/*Tim3*, *Lag3*, *Cd70*), and transcription factors (*Batf3*, *Zeb2*, *Nr4a3*), suggesting their critical roles in regulating recall responses. Notably, the previous human study identified distinct poised genes (*ID2*, *SLA*, *NFIL3*) and bivalent genes (*MLK4*, *MKX*, *GJB7*) in central memory and/or effector memory human CD8$^+$ T cells[11]. It should be noted that *CD70*, *FAM129A*, *IFNG*, *NR4A3*, *TNF*, *TNFRSF4*, *TNFSF14* and *TNIP3* classified as active genes in resting human memory CD8$^+$ T cells compared to resting naïve cells in the previous study were identified in our study as ARGs, based on their enhanced recall kinetics (faster/stronger induction) upon stimulation. Thus, our study specifically focuses on elucidating the epigenetic basis of the ARGs inherent to memory T cells.

A limitation of this study is the absence of subset-specific analysis within the CD8$^+$ memory T cell compartment, which encompasses $T_{CM}$, $T_{EM}$, and $T_{RM}$ populations. While recall response genes may exhibit subtle variations between subsets, existing evidence indicates that the core epigenetic features at these loci are largely conserved[11], suggesting a common regulatory mechanism. Indeed, our data demonstrate that both $T_{CM}$ and $T_{EM}$ exhibit highly similar induction patterns of ARGs compared to naïve cells (Supplementary Fig. 1d–f). Given the profound epigenetic and functional differences between memory and naïve T cells significantly outweigh the distinctions among memory subsets, this study focused on defining the general epigenetic landscape characterizing memory CD8$^+$ T cells as a population. Whether $T_{CM}$, $T_{EM}$, or $T_{RM}$ utilize subset-specific epigenetic mechanisms for recall responses remains an important question for future investigation.

While H2A.Z, a key epigenetic regulator, has been extensively characterized in diverse model systems[14,21,22], its specific functions in T cell development and immune responses remain poorly defined. Previous correlative studies linked H2A.Z deposition to gene expression in T cells[12,38,39], and we demonstrated its requirement for T cell proliferation via DNA replication licensing[27]. Here, we establish a novel role for H2A.Z in licensing the rapid recall response of memory T cells. To specifically interrogate this function and circumvent potential confounding effects on early T cell development or primary activation, we employed conditional knockout strategies: GzmB-Cre$^+$H2A.Z$^{f/f}$ mice, in which H2A.Z depletion occurs after naïve T cell primary activation, and Rosa26-creERT2$^+$H2A.Z$^{f/f}$ mice, in which H2A.Z depletion occurs after memory T cell establishment (tamoxifen-induced). Memory T cells generated from these models exhibited significantly impaired recall responses upon both in vitro antigen re-stimulation and in vivo infection re-challenge, as measured by defective effector cytokine production and reduced expansion. These results provide compelling genetic evidence that H2A.Z is essential for the rapid recall function of memory CD8$^+$ T cells.

H2A.Z may regulate cell expansion through both origin-recognition complex (ORC)-dependent and -independent mechanisms. Our data reveal that while the number of H2A.Z deposition peaks is comparable between memory and naïve CD8$^+$ T cells, the level of H2A.Z deposition is significantly higher in memory cells (Fig. 3a, b). This elevated deposition may prime memory T cells for enhanced recruitment of SUV420H1, increased H3K20me2 modification, and consequently greater ORC recruitment – potentially facilitating accelerated DNA replication and proliferation upon re-stimulation. However, this specific mechanism requires further experimental validation. Beyond direct DNA replication regulation, H2A.Z likely controls

https://doi.org/10.1038/s41467-025-62976-4

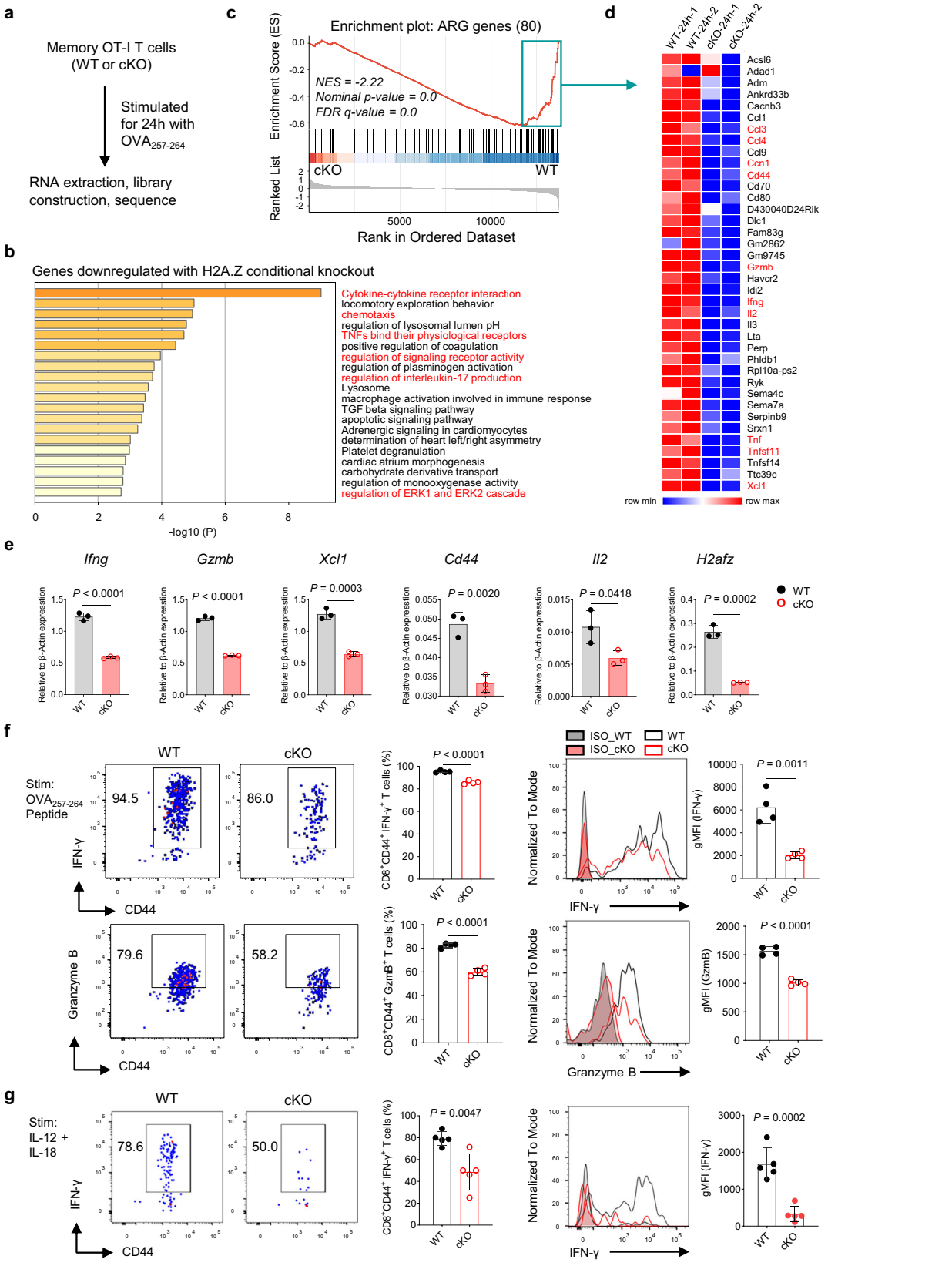


recall expansion via transcriptional regulation of key genes. Notably, several identified ARGs regulate lymphocyte proliferation. For instance, Batf3 has been reported to drive the expression of c-Myc[40], a critical transcription factor controlling T cell expansion. In addition, Zbtb32 has been reported to promote the proliferative burst of virus-specific natural killer cells responding to infection[41], though its effect in T cells remains to be clarified. Thus, H2A.Z likely primes memory T cells for rapid expansion by coordinately regulating both DNA replication licensing and the transcription of pro-proliferative genes.

H2A.Z establishes a permissive chromatin state for ARG transcription through multiple mechanisms: enhancing chromatin accessibility, facilitating histone modifications, and promoting RNA

**Fig. 5 | H2A.Z regulates the expression of activation-recalled genes in memory T cells. a**–**g** Naïve OT-I cells sorted from the spleens of WT (OT-I H2A.Z$^{f/f}$) or cKO (OT-I H2A.Z$^{f/f}$ GzmB-Cre) mice were transferred into hosts followed by LM-OVA infection. Day30-45 post-infection $T_M$ (CD127$^{hi}$KLRG1$^{lo}$) cells were sorted from spleens. **a** Experiment setup. WT and cKO $T_M$ cells were stimulated in vitro with 200 nM $OVA_{254-264}$ for 24 h, RNA was extracted for transcriptome analysis ($n = 2$ biologically independent samples per group). **b** Functional enrichment analysis of $T_M$ activation-recalled genes. **c** Enrichment plots of defined ARG gene set in comparison of cKO versus WT CD8$^+$ $T_M$ cell transcriptomes with GSEA. **d** Heatmap of selected genes from ARGs. **e** qPCR analysis of *Ifng*, *Gzmb*, *Xcl1*, *Prf1*, *Cd44*, *Il2*, and *H2afz* mRNA levels in WT and cKO $T_M$ cells stimulated with 2 μg/ml plate-bound anti-CD3/CD28 Abs for 24 h ($n = 3$ biologically independent samples per group). **f**, **g** The splenic cells from recipients were stimulated with $OVA_{257-264}$ peptide or a combination of IL-12 and IL-18. **f** IFN-γ and Granzyme B production from OT-I cells was measured by flow cytometry. Representative flow plots show the frequency of CD44$^+$IFN-γ$^+$ (top) and CD44$^+$ Granzyme B$^+$ (bottom) cells upon 24 h peptide stimulation ($n = 4$ biologically independent samples per group). **g** Representative flow plots show the frequency of CD44$^+$IFN-γ$^+$ cells upon 6 h IL-12/IL-18 stimulation ($n = 5$ biologically independent samples per group). Data are representative of two independent experiments in (**b**–**g**). Data are mean ± SD. Statistical analysis was performed using two-tailed unpaired Student's t test (**e**–**g**).

polymerase II recruitment. This functional versatility stems from at least two fundamental properties. First, intrinsic nucleosome destabilization: Compared to canonical H2A, H2A.Z possesses a shorter C-terminal tail deficient in positively charged residues[42], reducing its DNA-binding affinity. This lowers the energy barrier for DNA unwrapping in H2A.Z-containing nucleosomes, a mechanism corroborated by single-particle cryo-EM studies revealing enhanced C-terminal tail flexibility[16]. These biochemical properties intrinsically promote higher DNA accessibility. Second, recruitment of chromatin regulators: H2A.Z interacts with diverse protein complexes. It associates with ISWI chromatin remodelers (SMARCA5 and SMARCA1)[43], which enhance accessibility and facilitate transcription factor binding[44,45]. H2A.Z also recruits MLL complexes[46], that catalyze H3K4me3 methylation, a conserved activation mark[47]. Consistently, H2A.Z knockdown reduces binding of the core MLL subunit RbBP5[20]. While these mechanisms are central, we cannot exclude additional pathways. Notably, 3D chromatin reorganization has been linked to memory recall responses[48,49]. Through enhanced factor recruitment and accessibility, H2A.Z may facilitate structural changes in chromatin architecture[22], licensing rapid transcriptional induction. Beyond ARGs, H2A.Z broadly occupies other inducible genes (Supplementary Fig. 11e) and modulates their expression[12,39], consistent with its genome-wide distribution. However, genes exhibit differential regulatory dependence on H2A.Z. Given H2A.Z's complexity, including isoforms, post-translational modifications, and nucleosomal contexts[14,21,22,50], we postulate that specialized H2A.Z states (e.g., specific isoforms or modifications) may be essential for the rapid, robust induction of ARGs, contrasting with the slower, moderate induction of other H2A.Z-associated genes. This compelling hypothesis warrants detailed future investigation.

Epigenetic changes are not autonomous processes. Consequently, a key question is how the H2A.Z-dependent chromatin landscape characteristic of memory T cells is established. Given the profound epigenetic differences between naïve and memory T cells, we hypothesized that recall-associated changes are likely induced by extrinsic signals encountered during differentiation from naïve to memory T cells. To identify these signals and assess their direct, early effects, we employed a simplified in vitro short-term stimulation model. This approach revealed that both TCR/CD28 signaling and IL-7/IL-15 cytokine signaling regulate H2A.Z deposition: TCR/CD28 stimulation alone induced substantial H2A.Z deposition, while the addition of IL-7/IL-15 signals further modified H2A.Z levels, indicating synergistic regulation by these pathways. These findings suggest that T cells epigenetically encode their signal history to license enhanced recall responses. However, the long-term stability of this signal-induced H2A.Z deposition and the mechanisms governing its maintenance during memory T cell quiescence remain unknown.

How is H2A.Z specifically deposited at ARG loci? While general H2A.Z deposition mechanisms are largely known[21], the factors determining locus-specific targeting remain unclear. Motif analysis of H2A.Z binding sites within ARG loci identified consensus TF binding sequences, suggesting TF-dependent H2A.Z recruitment. To test this hypothesis and minimize functional redundancy among TFs, we mutated some consensus TF binding motifs within the *Ifng* locus using CRISPR/Cas9 in EL4 cells and primary murine T cells. The mutations significantly reduced H2A.Z deposition at the target sites and impaired subsequent *Ifng* induction upon re-stimulation.

In conclusion, we have identified H2A.Z as an essential epigenetic regulator licensing the rapid recall response of memory CD8$^+$ T cells. TCR/CD28 and IL-7/IL-15 cytokine signals, acting during memory differentiation, cooperatively establish this H2A.Z-dependent poised chromatin landscape. Pharmacologically targeting this pathway represents a promising strategy for enhancing vaccine efficacy and T cell-based immunotherapies.

## Methods

### Study design

The objective of this study was to define the role of H2A.Z in memory CD8$^+$ T cell recall response. In vivo studies were conducted in mice. In vitro studies involved primary mouse cells. Multiple experimental techniques were used, including flow cytometry, RNA-seq, ATAC-seq, ChIP-seq, and CUT&Tag analysis. Males and females were used in these experiments.

### Animals

OT-I (Jackson Laboratory, Stain #003831) is a C57BL/6 TCR transgenic strain[51], expressing a receptor specific for peptide $OVA_{257-264}$ in the context of H2-K$^b$. H2A.Z$^{f/f}$ mice[52] (RIKEN Center, RBRC05765) were kindly provided by Guohong Li (Institute of Biophysics, Chinese Academy of Sciences, Beijing, China). GzmB-Cre mice[26] originated from JAX Lab (Stain #003734) were kindly provided by Qibin Leng (Guangzhou Medical University, Guangzhou, China). Rosa26 ERT2-cre mice[28] originated from JAX lab (Strain #008463) were kindly provided by Bo Zhong (Wuhan University, Wuhan, China). Ly5.1 (Stain #002014) transgenic mice were obtained from Jackson Laboratory. All mice mentioned above were housed and bred in specific-pathogen-free (SPF) facilities under a 12-hour light/12-hour dark cycle, at temperatures ranging from 20 to 26°C and relative humidity between 40% and 70%, with ad libitum access to water and food. All animal experimental procedures were performed with approval (SYXK2020035 and ABSL-2-2021006) from the institutional committee of the Institute of Biophysics, Chinese Academy of Sciences. Both experimental and control mice were co-housed and bred together before separating. Mice are euthanized by carbon dioxide ($CO_2$) inhalation using the euthanasia chamber, and double verified the death by ascertaining cardiac and respiratory arrest.

### Cell culture

T cells were maintained in RPMI 1640 (Gibco) supplemented with 10% fetal bovine serum (BI), 10 mM Hepes (Gibco), 1% NEAA (Gibco), 1% penicillin/streptomycin (Gibco), 50 μM β-Mercaptoethanol (Gibco) in humidified atmosphere with 5% CO2 at 37 °C. EL-4 mouse lymphoma cell line (ATCC) and Phoenix-ECO cells (ATCC) were maintained in DMEM containing 10% fetal bovine serum, 10 mM Hepes and 1% penicillin/streptomycin.

https://doi.org/10.1038/s41467-025-62976-4

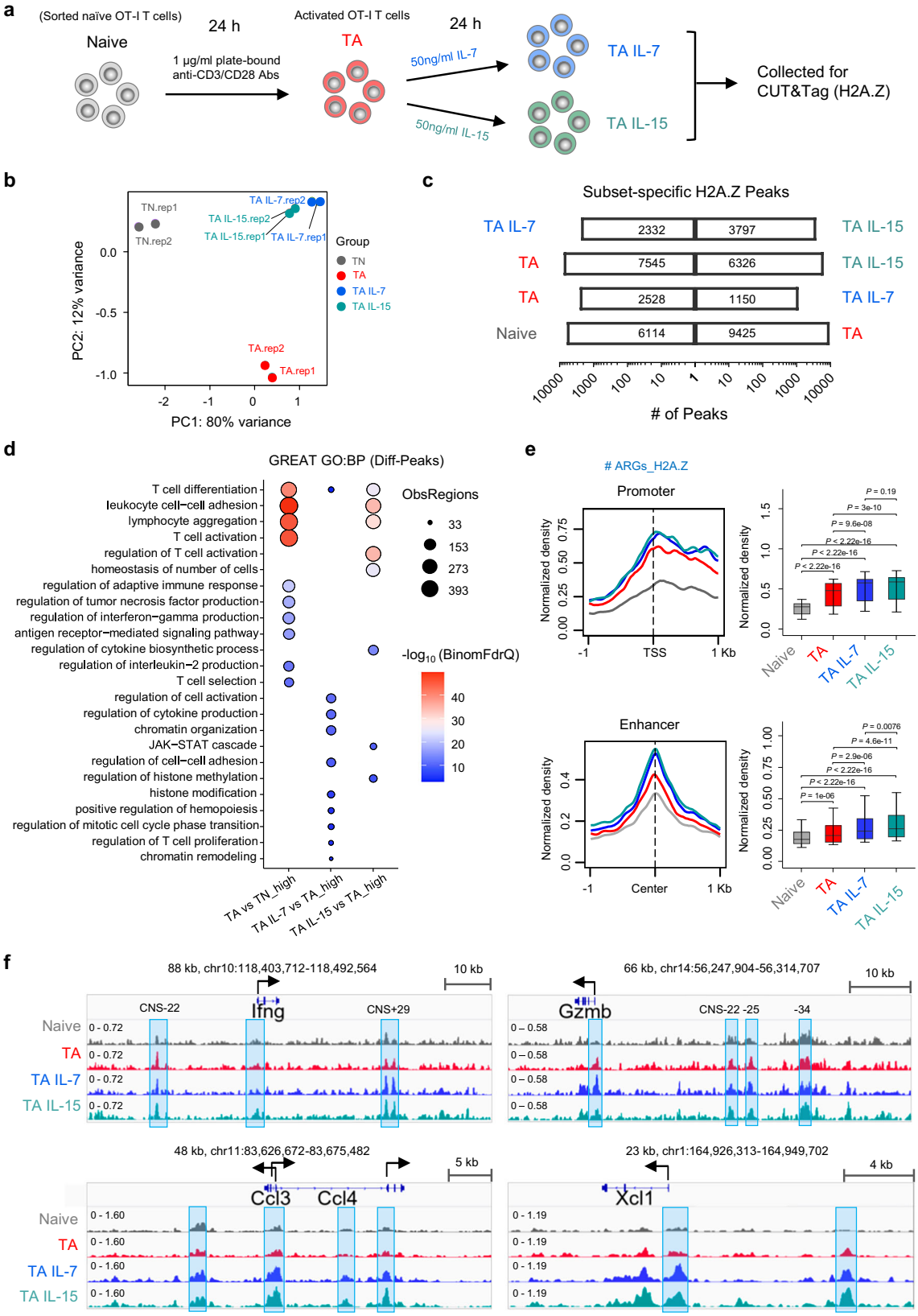


## Adoptive transfer model

To detect primary T cell proliferation in vivo, wild-type (WT) and H2A.Z$^{f/f}$ GzmB-Cre (cKO) naïve OT-I T cells were purified by FACS, labeled with 5 μM CFSE (ThermoFisher, Cat. No. C34554), and co-transferred (mixed at a 1:1 ratio, $5 \times 10^6$ per mouse) to the congenically marked recipients. On the next day, the recipients were intravenously (i.v.) infected with $5 \times 10^3$ CFU of LM-OVA. At 3–7 days post-infection, the proliferation of donor cells was detected. To generate WT and cKO memory OT-I cells, wild-type (WT) and H2A.Z$^{f/f}$ GzmB-Cre (cKO) naïve OT-I T cells were purified by FACS, separately transferred or co-transferred (mixed at a 1:1 ratio, 1.5 to $2 \times 10^5$ per mouse) to the congenically marked recipients. On the next day, the recipients were

**Fig. 6 | TCR/CD28 and cytokine signals induce H2A.Z deposition at specific gene loci. a** Experiment setup. Naïve OT-I cells were stimulated by 1 μg/ml plate-bound anti-CD3/CD28 Abs for 24 h (Activated T cells, TA), and then stimulated with 50 ng/ml IL-7 or IL-15 for another 24 h, respectively. The cells were collected at different steps for H2A.Z CUT&Tag-seq ($n = 2$ biologically independent samples per group). Data are representative of two independent experiments. **b** Principal components analysis (PCA). **c** Quantification of differential H2A.Z peaks ($p$-value < 0.01; |M value | > 1) between subsets on a logarithmic scale (across genome-wide regions). **d** Network analysis (GREAT) of biological-process GO term enrichment of the genes with unique H2A.Z-deposited peaks induced by changes in TCR/CD28, TCR/CD28 + IL-7 or TCR/CD28 + IL-15 signals. Top GO biological processes terms and −log10 BinomFdrQ (binomial FDR $q$-value) are shown. **e** The Figure shows th**e** density of peaks around TSS (upper panel, promoter regions) and enhancer regions (lower panel). Box plots showing signal strength of ARGs loci in Naive, TA, TA IL-7, and TA IL-15 using normalized read counts of H2A.Z CUT&Tag-seq peaks in each condition. Statistical significance was determined with two-sided paired Wilcoxon test. **f** Sequencing tracks at selected gene loci as displayed on the IGV, with gene structure and transcription orientation marked on the top.

intravenously (i.v.) infected with $5 \times 10^3$ CFU of LM-OVA. At 30–45 days post-infection, WT and cKO memory OT-I cells were sorted for in vitro activation or transferred into the congenically marked recipients for recall response detection. To generate WT and icKO memory OT-I T cells, OT-I wild-type (WT) and H2A.Z$^{f/f}$ Rosa26 ERT2-cre (icKO) naïve T cells were purified by FACS, separately transferred or co-transferred (mixed at a 1:1 ratio, 1.5 to $2 \times 10^5$ per mouse) to the congenically marked recipients. On the next day, the recipients were i.v. infected with $5 \times 10^3$ CFU of LM-OVA. On day 30, tamoxifen (TAM) was injected intraperitoneally at 100 mg/kg for 5 consecutive days. On day 10 following TAM injection, WT and icKO memory OT-I cells were sorted for in vitro activation or transferred into the congenically marked recipients for recall response detection. For comparison of naïve and memory T cell response, OT-I naïve (day 0) and memory T cells (at 30–45 days post-infection) were purified by FACS, mixed at a 1:1 ratio, and co-transferred into the congenically marked recipients (2 to $4 \times 10^4$ cells per recipient). One day after the transfer, mice were i.v. infected with $1 \times 10^5$ CFU of LM-OVA and 4 and/or 7 days later, OT-I T cell response were analyzed. For secondary infection experiments, WT and cKO or WT and icKO memory OT-I T cells were purified by FACS from primary recipients at 30–45 days post-infection, mixed in a 1:1 ratio, and co-transferred into the congenically marked recipients (2 to $4 \times 10^4$ cells per recipient), followed by i.v. infection with $1 \times 10^5$ CFU of LM-OVA. On day 4 and/or 7 post-infection, the recall responses were measured. Antibodies used for FACS are listed in Supplementary Table 2.

### Listeria monocytogenes infection

*Listeria monocytogenes* expressing the chicken ovalbumin (LM-OVA) was a kind gift from Yang-Xin Fu (University of Chicago). Bacteria were grown to a logarithmic phase in Brain Heart Infusion (BHI) medium (ThermoFisher, Cat. No. CM1135B). For the study of primary immune response, mice were intravenously infected with $5 \times 10^3$ colony-forming units (CFU) of ovalbumin-expressing *Listeria monocytogenes* (LM-OVA). Mice that had received OT-I cells were intravenously infected with $5 \times 10^3$ CFU of LM-OVA 1 day after the adoptive T cell transfer. To analyze the secondary immune response, mice were rechallenged with $1 \times 10^5$ CFU of LM-OVA at day 30–45 after primary infection. The recall response was determined 4 and/or 7 days after the secondary infection.

### RNA extraction

RNA was extracted by Easy Pure RNA Kit (Transgen, Cat. No. ER101). Add BB4 (containing β-mercaptoethanol) from the kit to fully lyse the cells, followed by ethanol precipitation, purification column adsorption, washing, and removal of genomic DNA with DNase I. Finally, 30 μl of RNase-free dd$H_2O$ was added for RNA elution. RNA concentration was measured with Nanodrop, and an appropriate amount of RNA was used for reverse transcription or RNA library construction. RNA was stored at −80 °C.

### qPCR

For reverse transcription of RNA samples, Thermo Fisher Reverse Transcription Kit (Cat. No. EN032) was used. The RT-PCR reagents used were SYBR Green Mix from Takara Company, and a 96-well plate reaction was conducted using the ABI QuantStudio 6. Relative mRNA expression was calculated with the $2^{-\Delta\Delta CT}$ method. The internal reference gene selected is the housekeeping gene *Actb* (beta-actin).

### Flow cytometric analysis

Cells were incubated with an anti-CD16/CD32 (2.4G2) mAb to block Fcγ receptors and then stained on 4 °C for 30 min with several combinations of mAbs. DAPI (1000 × dilution) was added before detection to distinguish between dead and alive cells. Flow cytometry was performed on a LSRFortessa cytometers (BD), and the data were analyzed with the Flowjo software (Treestar, San Carlos, CA). Cell sorting was performed on FACSAria instruments (BD). Intracellular staining was performed with eBioscience Foxp3/Transcription Factor Staining Buffer Kit (Cat. No. 00-5523-00). Cell apoptosis was quantified by using the APC Annexin V Apoptosis Detection Kit (Biolegend, Cat. No. 640932) and 7-AAD (eBioscience, Cat. No. 00-6993-50) according to the manufacturer's instructions. Briefly, the testing cells were harvested and washed with cold Cell Staining Buffer (Biolegend, Cat. No. 420201). Cell density was adjusted to $1 \times 10^6$ cells/100 μl in 1× Annexin V binding buffer and stained with Annexin V-APC and 7-AAD for 15 min at room temperature.

### Immunoblotting

T cells were sorted and lysed in lysis buffer (10 mM Tris-HCl, 1 mM EDTA, 1% SDS), containing Protease Inhibitor Cocktail (Beyotime, Cat. No. P1006). The cell lysates were extracted and electrophoresed on 12.5 or 15 % polyacrylamide gels. After electrophoresis at 120 V for 30 min, proteins were transferred to PVDF membranes. Membranes were blocked in 5% BSA in TBS-T (10 mM Tris−HCl, 150 mM NaCl, and 0.1% Tween 20) at room temperature for 1 h, and then incubated with the following antibodies: anti-H2A.Z (Abcam, Cat. No. ab4174) and anti-β-Actin (Zsbio, TA-09) in 3 % BSA in TBS-T overnight at 4 °C. After washing, the membranes were covered with the HRP-labeled secondary Ab at room temperature for 1 h, and visualized with Ultra High Sensitivity ECL Kit (MCE, Cat. No. HY-K1005). Images were captured by GenoSens 2000 System (Clinx, Shanghai, China). Densitometric quantitation of bands was performed using ImageJ 1.54 f software.

### RNA-seq and computational analysis

For naïve and memory OT-I cell activation, $2 \times 10^5$ T cell were inoculated with 2 μg/ml plate-bound anti-CD3 Ab (Biolegend, Cat. No. 100340) and 1 μg/ml soluble anti-CD28 Ab (Biolegend, Cat. No. 102116) for 0, 6 or 24 h in 96-well plate. After treatment, RNA was isolated from the T cells using EasyPure RNA Kit (TransGen Biotech, Cat. No. ER101-01). For WT and cKO memory OT-I cell activation, $1 \times 10^5$ cells per well were stimulated with 200 nM $OVA_{257\text{-}264}$ peptide in a 96-well plate. After 24 h stimulation, RNA was isolated from the T cells using HiPure Total RNA Nano Kit (Magen, Cat. No. R4125-02). RNA libraries for RNA-seq were prepared using TruePrep RNA Library Prep Kit for Illumina (Vazyme, Cat. No. TR502-02) following manufacturer's protocols. Sequencing was performed on an Illumina NovaSeq 6000 or NovaSeq X Plus instrument (150 bp, paired-end) at Berry Genomics Co., Ltd. (Beijing, China). Trim Galore (v0.6.7) and Trimmomatic (v0.39) was used to filter out low-quality reads. STAR (v2.7.9a) was used to align reads to the mouse genome. RSEM

https://doi.org/10.1038/s41467-025-62976-4

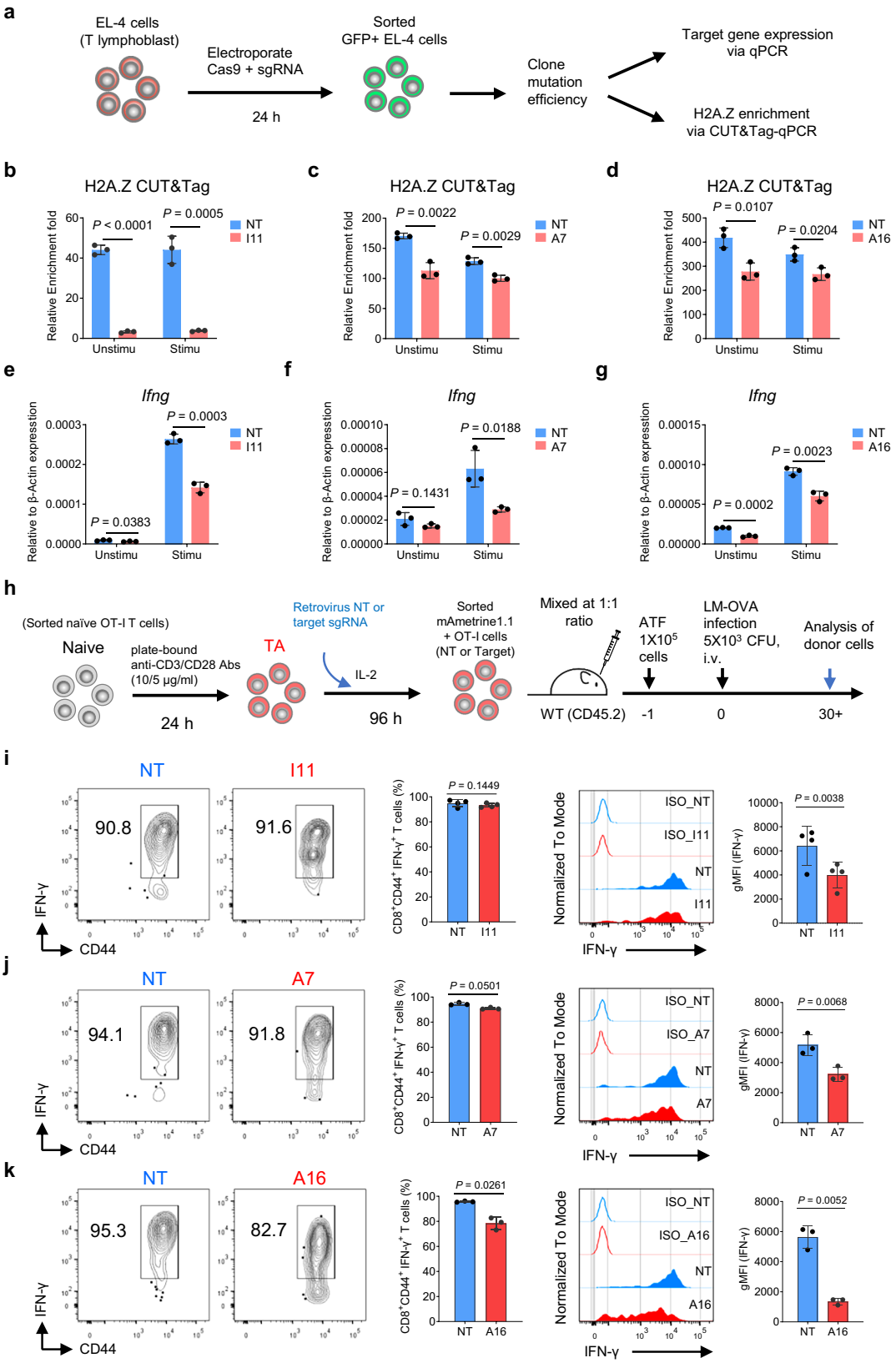


(version 1.3.1) with the command rsem-calculate-expression was used to calculate the FPKM values for gene expression in each sample. Memory T cell activation-recalled genes (ARGs) were defined by [1] increase of mRNA expression in activated over resting memory cells by at least 4-fold, [2] increase of mRNA expression in activated over resting naïve cells by at least 4-fold, [3] increase of mRNA expression in activated memory T over activated naïve T cells by at least 2-fold, [4] *P*-value < 0.01. Silent genes had FPKM < 2 in resting and activated memory T cells. Memory T cell activation-induced genes (AIGs) were defined by [1] increase of mRNA expression in activated over resting memory cells by at least 4-fold, [2] FPKM > 5 in resting and activated memory T cells, [3] *P*-value < 0.01.

**Fig. 7 | Multiple TFs regulate H2A.Z enrichment at effector gene loci and contribute to their expression. a** Experiment setup. EL-4 cells were electroporated with EGFP-lentiCRISPRv2_sgRNA plasmid. 24 h post-electroporation, GFP$^+$ cells were sorted and collected for DNA sequencing. DNA modifications were quantified using TIDE. **b**–**g** The GFP$^+$ cells were cultured in 1 μg/ml plate-bound anti-CD3/CD28 Abs for 24 h and then collected for CUT&Tag (**b**–**d**) and qPCR (**e**–**g**). Data from three biologically independent samples (**e**–**g**). **h** Experiment setup. **h**–**k** Activated OT-I cells were transduced with Retrovirus system. 96 h post-transduction, NT and target GFP$^+$ cells were sorted and mixed at a 1:1 ratio and co-transferred into recipients. On the next day, these mice were infected with $5 \times 10^3$ CFU LM-OVA. On day 30-45, the splenic cells from recipients were stimulated with PMA/Ionomycin for 4 h. IFN-γ production from OT-I cells was measured by flow cytometry. Values denote geometric mean fluorescence intensity (gMFI). Data from four (**i**) or three (**j**, **k**) biologically independent samples. Data are representative of two independent experiments in (**b**–**g** and **i**–**k**). Data are mean ± SD. Statistical analysis was performed using two-tailed unpaired Student's t test (**b**–**g**) and two-tailed paired Student's t test (**i**–**k**).

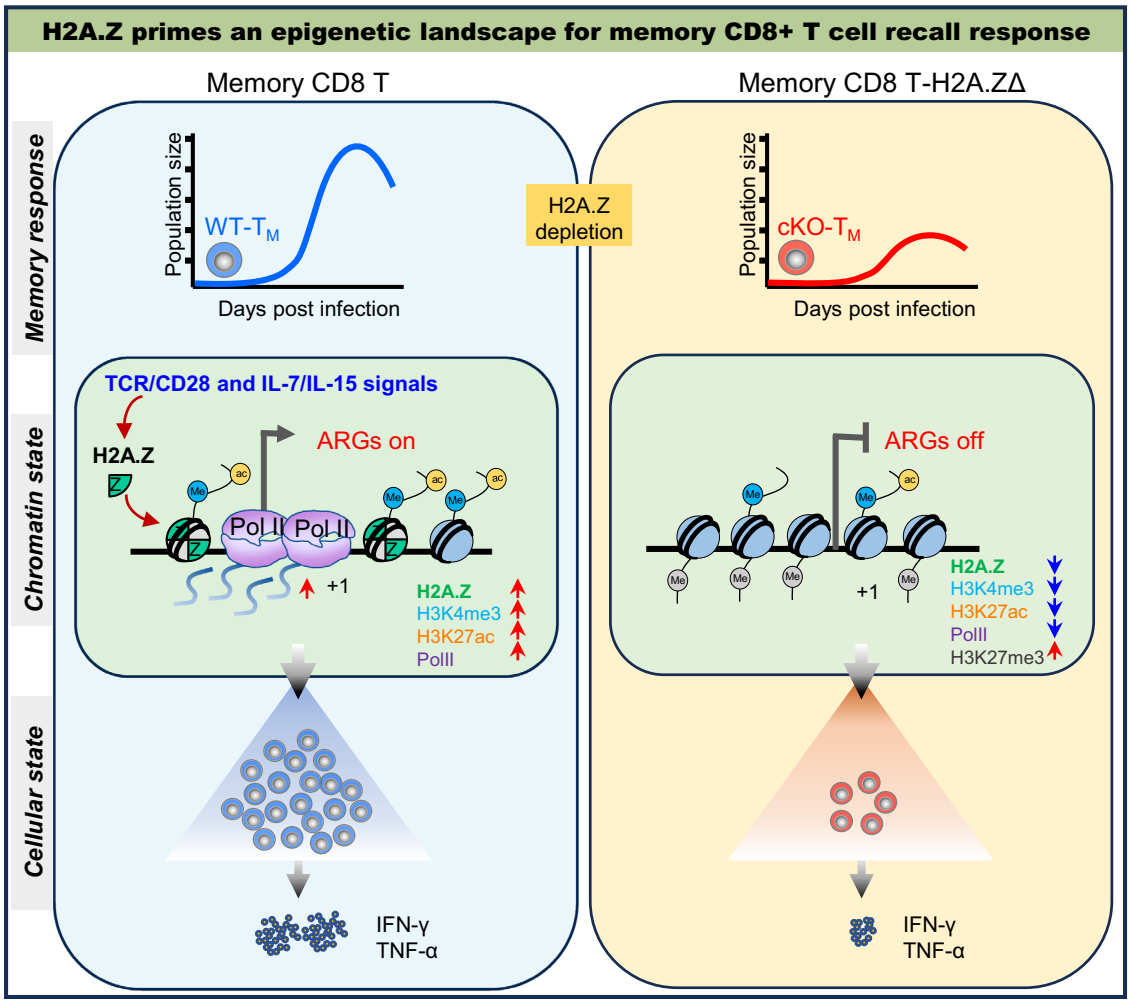


**Fig. 8 | Schema of H2A.Z primes an epigenetic landscape for memory CD8$^+$ T cell recall response.** Resting memory T cells exhibit a poised chromatin landscape at activation-recalled genes (ARGs). H2A.Z is required for memory CD8$^+$ T cell recall response. H2A.Z sets up the poised chromatin landscape on the promoters, typical and super enhancers of ARGs for their recall expression. TCR/CD28 and IL-7/IL-15 signals cooperate to promote H2A.Z deposition at specific ARG loci.

### ATAC-seq and computational analysis

$4 \times 10^4$ memory OT-I T cells derived from WT or cKO mice were used to assess the chromatin accessibility by ATAC-seq (Assay for Transposase-Accessible Chromatin with high-throughput sequencing) technology. The TruePrep DNA Library Prep Kit V2 for Illumina (Vazyme, Catalog No. TD501-01) was utilized according to the manufacturer's instructions to prepare the sequencing libraries. The Trim Galore software was used for quality control of ATAC-seq raw data, filtering out sequencing fragments less than 20 bp in length. The genome comparison software used is bowtie2 v2.5.1[53]. After comparison, MarkDuplicates in Picard was used to remove redundant comparison results. For quality control of BAM files after comparison, please refer to the official documentation of ENCODE. Before peak analysis, the BAM file needs to be shifted according to the occupancy of the Tn5 enzyme. This operation is completed by alignmentSieve in deepTools v3.4.3[54]. Read visualization is completed using IGV software[55]. The bamCoverage function needs to be used to generate the bigwig format Input file, and RPKM is selected as the standardization method. The Peak calculation software used is MACS2 v2.2.7.1[56], with the threshold set at $q$-value < 0.05. Peak count calculation is implemented using the featureCounts function of Subread v1.6.2[57] software. Peak annotation was completed using the ChIPseeker package.

### Native ChIP-seq and computational analysis

Chromatin immunoprecipitation refers to the ULI-NChIP method published by Brind'Amour Julie et al[58]. Native ChIP-seq was used to conduct a detailed analysis of histone H3K27 acetylation (H3K27ac) in memory CD8$^+$ T cells originating from WT and cKO mice to compare

their distribution characteristics on H2A.Z-regulated gene sites. Antibodies used for native ChIP are listed in Supplementary Table 3. For ChIP-seq, Trim Galore software was used to perform quality control on the raw data, sequencing fragments less than 20 bp in length was filtered out. The genome alignment software used is bowtie2. After alignment, MarkDuplicates in Picard is utilized to remove redundant alignment results, followed by the use of samtools v1.10[59] to eliminate reads with MAPQ < 10. Read visualization is carried out using IGV software. It is necessary to utilize the bamCompare function to generate bigwig format input files, with RPKM selected as the standardization method. The Peak calculation software employed is MACS2, with the threshold set at $q$-value < 0.05. The count number calculation of the Peak is implemented using the featureCounts function of the Subread (http://subread.sourceforge.net) software. Peak difference analysis is conducted using the DESeq2 software. During the calculation process, the Drosophila dm6 version is selected as the Spike-in genome to calculate the scale factor between different mouse samples. The difference threshold is set to |FoldChange| > 2 and padj <0.05. Peak annotation is completed using the ChIPseeker package[60]. Utilize the bigwig file as input, employ the computeMatrix function of deepTools software[54] to calculate the density value of the transcript in each region, and use the ggplot2 package for drawing display.

### CUT&Tag and computational analysis

CUT&Tag assay was performed using the Hyperactive Universal CUT&Tag Assay Kit for Illumina Pro (Vazyme, Cat. No. TD904-02) following the manufacturer's instructions. Briefly, a total of $4 \times 10^4$ freshly sorted naïve or memory OT-I T cells were tagged with concanavalin A-coated magnetic beads and then incubated with 1 μg of primary antibody [rabbit polyclonal anti-Histone H2A.Z, anti-H3K4me3, anti-H3K27me3, anti-H3K27ac, anti-RNA polymerase II CTD repeat YSPTSPS (phospho S5)] overnight at 4 °C with slow rotation. Antibodies used for CUT&Tag are listed in Supplementary Table 3. After incubated with 1 μg secondary antibody (goat anti-rabbit IgG H&L) at room temperature for 1 hour, cells were incubated with 0.04 μM Hyperactive pG-Tn5 Transposon and then resuspended in tagmentation buffer for tagmentation. DNA was purified and amplified by 12 to 14 PCR cycles to generate the libraries. Libraries were sequenced on Illumina Nova-PE150, and 150-bp paired-end reads were generated. For CUT&Tag qPCR detection, 5 μl of Stop Buffer was added to extract DNA after tagmentation. Using the negative control (IgG) as a control, calculate the 2^(-ΔΔCT) values for each group to determine the relative enrichment fold: Relative Enrichment fold (treatment)= 2-(ΔCT treatment (CT treatment − CT treatment DNA Spike-in)− ΔCT IgG (CT IgG − CT IgG DNA Spike-in)); Relative Enrichment fold (control) = 2-(ΔCT control (CT control − CT control DNA Spike-in) − ΔCT IgG (CT IgG − CT IgG DNA Spike-in)).

For data processing, raw sequencing data were trimmed and filtered by using Trim Galore. Bowtie2 (v2.5.1) was used to align reads to the mouse reference genome mm10 with default parameters and then sorted using the Samtools (v1.15). MACS2 (v2.2.7.1) was used to call peaks. bamCoverage (v3.5.1) was used to generate bigwig files from bam files. The distribution of CUT&Tag peaks was annotated with the R package ChIPseeker.

### Enhancers were stitched and super-enhancers were identified using ROSE

The ROSE_main.py function from ROSE[30,31] was used to identify typical- or super-enhancers based on H3K27ac ChIP-seq signals, with the parameters '-s 12,500 -t 2500'. Enhancers were annotated to their nearest genes using the ROSE_geneMapper.py function. ROSE_geneMapper.py function was used to annotate enhancers by their nearest genes. H2A.Z-enriched ARG gene regions were then intersected with the annotated enhancer regions. Among the 80 ARGs, 42 gene-related enhancers were analyzed.

### Pathway enrichment analysis

For functional annotation of GO and KEGG pathway enrichment was performed by Metascape (https://metascape.org)[61]. Differential peaks were analyzed using the Gene Regional Enrichment of Annotations Tool (GREAT)[35] for GO biological processes enrichment. The results from GREAT were visualized as enrichment plot through ImageGP[62].

### CRISPR Cas9 targeting

sgRNAs were designed by using the online tool (https://crispor.gi.ucsc.edu/) and subsequently cloned into LentiCRISPRv2GFP vector (Addgene, Cat. No. 82416). The lentiviral sgRNA vector were electroporated into EL-4 cells. After 24 h electroporation, $GFP^+$ cells were sorted and collected for DNA sequencing. DNA modifications were quantified using TIDE. The $GFP^+$ cells were cultured in 1 μg/ml plate-bound anti-CD3/CD28 Abs for 24 h and then collected for CUT&Tag and qPCR. Oligonucleotide sequences used for EGFP-lentiCRISPRv2_sgRNA plasmid and CUT&Tag-qPCR are listed in Supplementary Table 4.

### Retrovirus based CRISPR Cas9 targeting

The retroviral sgRNA vectors were previously described[37]. sgRNAs were cloned into retroviral vector, and then the retroviral sgRNA vector was co-transfected into Phoenix-ECO cells with the helper plasmid pCL-Eco (Addgene, Cat. No. 12371) to produce retrovirus. Naïve OT-I T cells were isolated from OT-I $Cas9^+$ mice using naïve $CD8^+$ T cell isolation kit (Stem Cell technologies, Cat. No. 19858) according to the manufacturer's instructions. Purified naïve $CD8^+$ T cells stimulated with plate-bound anti-CD3/CD28 Abs (10/5 μg/ml) for 24 h. Viral transduction was performed by spin-infection at 800 × g at 32 °C for 2 h with 8 μg/ml polybrene (Sigma, Cat. No. H9268-5G), followed by continued culture under the condition of 10 ng/ml IL-2. 96 h post-transduction, NT and target mAmetrine1.1$^+$ OT-I cells were sorted and mixed at a 1:1 ratio and co-transferred into recipients. On the next day, these mice were infected with $5 \times 10^3$ CFU LM-OVA. On day 30-45, the splenic cells from recipients were stimulated with PMA/Ionomycin for 4 h. IFN-γ production from OT-I cells was measured by flow cytometry.

### RNP ProteanFect System based gene editing

Human naïve $CD8^+$ T cells were isolated from frozen aliquots of PBMCs (Milestone Biotechnologies, Cat. No. PB050C) and activated in X-VIVO 15 Medium (Lonza, Cat. No. 02-060Q) containing 25 μl/ml of Human CD3/CD28 T Cell Activator (Stem Cell technologies, Cat. No. 10971) for four days. Subsequently, mRNA cocktails (which included H2A.Z.1 sgRNA, H2A.Z.2 sgRNA, EGFP mRNA, and Cas9 mRNA) were transfected into the activated human $CD8^+$ T cells using the ProteanFect CRISPRMax-Cas9 mRNA Gene Editing Kit (ProteanFect, Cat. No. PT05). After 24 h of transfection, $EGFP^+$ cells were sorted and subsequently cultured in the presence of IL-7 and IL-15 for 8 days. The transfected human $CD8^+$ T cells were then restimulated with Human CD3/CD28 T Cell Activator or PMA/Ionomycin for 4 h before being collected for flow cytometry analysis. The oligonucleotide sequences used for the sgRNAs are listed in Supplementary Table 4. The full-length sgRNAs (~100 nucleotides) were synthesized by Tsingke Biological Technology (Beijing, China).

### Statistical analysis

All statistical analyses were performed using Prism8 (GraphPad). The data were presented as mean ± SD, and a two-tailed Student's t test or two-sided paired Wilcoxon test were used as indicated in the Figure legends. The exact value of n (number of biological or experimental replicates) can be found in the Figure legends and the exact $P$ values were indicated in the graphed data. A $P$ value < 0.05 was considered statistically significant. Most experiments were carried out at least two or three times, and the findings of all key experiments were reliably reproduced.

### Reporting summary

Further information on research design is available in the Nature Portfolio Reporting Summary linked to this article.

## Data availability

All raw and processed High-throughput sequencing data generated in this work are publicly available at the Gene Expression Omnibus (GEO) data repository: RNA-Seq (GSE273103 [https://www.ncbi.nlm.nih.gov/geo/query/acc.cgi?acc=GSE273103], GSE273104 and GSE300170), ATAC-seq, CUT&Tag and ChIP-Seq (GSE273195 [https://www.ncbi.nlm.nih.gov/geo/query/acc.cgi?acc=GSE273195] and GSE273198). Previously published datasets used in this study were RNA-Seq data from Best et al[25]. for $CD8^+$ naïve and memory T cells (GSE15907 [https://www.ncbi.nlm.nih.gov/geo/query/acc.cgi?acc=GSE15907]). ATAC-seq, H3K4me3, H3K27me3 and H3K27ac in total $CD8^+$ naïve and memory T cells (GSE89036 [https://www.ncbi.nlm.nih.gov/geo/query/acc.cgi?acc=GSE89036])[24]. All data are included in the Supplementary Information or available from the authors, as are unique reagents used in this Article. The raw numbers for charts and graphs are available in the Source Data file whenever possible. Source data are provided with this paper.

## Code availability

No custom code or mathematical algorithms were used in this study. All analyses were conducted using established methods and standard software (see Methods). The code used to generate figures is available from the corresponding authors upon request.

## References


1. Gebhardt, T., Palendira, U., Tscharke, D. C. & Bedoui, S. Tissue-resident memory T cells in tissue homeostasis, persistent infection, and cancer surveillance. *Immunol. Rev.* **283**, 54–76 (2018).
2. Kallies, A., Zehn, D. & Utzschneider, D. T. Precursor exhausted T cells: key to successful immunotherapy? *Nat. Rev. Immunol.* **20**, 128–136 (2020).
3. Utzschneider, D. T. et al. T cell factor 1-expressing memory-like CD8(+) T cells sustain the immune response to chronic viral infections. *Immunity* **45**, 415–427 (2016).
4. Williams, M. A. & Bevan, M. J. Effector and memory CTL differentiation. *Annu. Rev. Immunol.* **25**, 171–192 (2007).
5. Gattinoni, L. et al. Wnt signaling arrests effector T cell differentiation and generates CD8+ memory stem cells. *Nat. Med.* **15**, 808–813 (2009).
6. Kaech, S. M. & Cui, W. Transcriptional control of effector and memory CD8+ T cell differentiation. *Nat. Rev. Immunol.* **12**, 749–761 (2012).
7. Kersh, E. N. et al. TCR signal transduction in antigen-specific memory CD8 T cells. *J. Immunol.* **170**, 5455–5463 (2003).
8. Lai, W. et al. Transcriptional control of rapid recall by memory CD4 T cells. *J. Immunol.* **187**, 133–140 (2011).
9. Henning, A. N., Roychoudhuri, R. & Restifo, N. P. Epigenetic control of CD8(+) T cell differentiation. *Nat. Rev. Immunol.* **18**, 340–356 (2018).
10. Weng, N. P., Araki, Y. & Subedi, K. The molecular basis of the memory T cell response: differential gene expression and its epigenetic regulation. *Nat. Rev. Immunol.* **12**, 306–315 (2012).
11. Araki, Y. et al. Genome-wide analysis of histone methylation reveals chromatin state-based regulation of gene transcription and function of memory CD8+ T cells. *Immunity* **30**, 912–925 (2009).
12. Barski, A. et al. Rapid recall ability of memory T cells is encoded in their epigenome. *Sci. Rep.* **7**, 39785 (2017).
13. Biterge, B. & Schneider, R. Histone variants: key players of chromatin. *Cell Tissue Res.* **356**, 457–466 (2014).
14. Subramanian, V., Fields, P. A. & Boyer, L. A. H2A.Z: a molecular rheostat for transcriptional control. *F1000prime Rep.* **7**, 01 (2015).
15. Thakar, A. et al. H2A.Z and H3.3 histone variants affect nucleosome structure: biochemical and biophysical studies. *Biochemistry* **48**, 10852–10857 (2009).
16. Lewis, T. S., Sokolova, V., Jung, H., Ng, H. & Tan, D. Structural basis of chromatin regulation by histone variant H2A.Z. *Nucleic Acids Res.* **49**, 11379–11391 (2021).
17. Ávila-López, P. A. et al. Interplay between the histone variant H2A.Z and the epigenome in pancreatic cancer. *Arch. Med. Res.* **53**, 840–858 (2022).
18. Liu, X. et al. Hierarchical accumulation of histone variant H2A.Z regulates transcriptional states and histone modifications in early mammalian embryos. *Adv. Sci.***9**, e2200057 (2022).
19. Brunelle, M. et al. The histone variant H2A.Z is an important regulator of enhancer activity. *Nucleic Acids Res.* **43**, 9742–9756 (2015).
20. Hu, G. et al. H2A.Z facilitates access of active and repressive complexes to chromatin in embryonic stem cell self-renewal and differentiation. *Cell Stem Cell* **12**, 180–192 (2013).
21. Giaimo, B. D., Ferrante, F., Herchenröther, A., Hake, S. B. & Borggrefe, T. The histone variant H2A.Z in gene regulation. *Epigenet. Chromatin* **12**, 37 (2019).
22. Colino-Sanguino, Y., Clark, S. J. & Valdes-Mora, F. The H2A.Z-nucleosome code in mammals: emerging functions. *Trends Genet. TIG* **38**, 516 (2022).
23. Shan, Q. et al. Tcf1 preprograms the mobilization of glycolysis in central memory CD8(+) T cells during recall responses. *Nat. Immunol.* **23**, 386–398 (2022).
24. Yu, B. et al. Epigenetic landscapes reveal transcription factors that regulate CD8+ T cell differentiation. *Nat. Immunol.* **18**, 573–582 (2017).
25. Best, J. A. et al. Transcriptional insights into the CD8(+) T cell response to infection and memory T cell formation. *Nat. Immunol.* **14**, 404–412 (2013).
26. Jacob, J. & Baltimore, D. Modelling T-cell memory by genetic marking of memory T cells in vivo. *Nature* **399**, 593–597 (1999).
27. Long, H. et al. H2A.Z facilitates licensing and activation of early replication origins. *Nature* **577**, 576–581 (2020).
28. Ventura, A. et al. Restoration of p53 function leads to tumour regression in vivo. *Nature* **445**, 661–665 (2007).
29. Li, X., Chu, V. T., Kocks, C. & Rajewsky, K. Expansion and precise CRISPR-Cas9 gene repair of autologous T-memory stem cells from patients with T-cell immunodeficiencies. *Bio-Protoc.* **14**, e5085 (2024).
30. Whyte, W. A. et al. Master transcription factors and mediator establish super-enhancers at key cell identity genes. *Cell* **153**, 307–319 (2013).
31. Lovén, J. et al. Selective inhibition of tumor oncogenes by disruption of super-enhancers. *Cell* **153**, 320–334 (2013).
32. Creyghton, M. P. et al. Histone H3K27ac separates active from poised enhancers and predicts developmental state. *Proc. Natl Acad. Sci. USA* **107**, 21931–21936 (2010).
33. Raeber, M. E., Zurbuchen, Y., Impellizzieri, D. & Boyman, O. The role of cytokines in T-cell memory in health and disease. *Immunol. Rev.* **283**, 176–193 (2018).
34. Chin, S. S. et al. T cell receptor and IL-2 signaling strength control memory CD8(+) T cell functional fitness via chromatin remodeling. *Nat. Commun.* **13**, 2240 (2022).
35. McLean, C. Y. et al. GREAT improves functional interpretation of cis-regulatory regions. *Nat. Biotechnol.* **28**, 495–501 (2010).
36. Atsaves, V., Leventaki, V., Rassidakis, G. Z. & Claret, F. X. AP-1 transcription factors as regulators of immune responses in cancer. *Cancers* **11**, 1037 (2019).
37. Long, L. et al. CRISPR screens unveil signal hubs for nutrient licensing of T cell immunity. *Nature* **600**, 308–313 (2021).

38. Barski, A. et al. High-resolution profiling of histone methylations in the human genome. *Cell* **129**, 823–837 (2007).
39. Schones, D. E. et al. Dynamic regulation of nucleosome positioning in the human genome. *Cell* **132**, 887–898 (2008).
40. Jain, N. et al. TET2 guards against unchecked BATF3-induced CAR T cell expansion. *Nature* **615**, 315–322 (2023).
41. Beaulieu, A. M., Zawislak, C. L., Nakayama, T. & Sun, J. C. The transcription factor Zbtb32 controls the proliferative burst of virus-specific natural killer cells responding to infection. *Nat. Immunol.* **15**, 546–553 (2014).
42. Li, S., Wei, T. & Panchenko, A. R. Histone variant H2A.Z modulates nucleosome dynamics to promote DNA accessibility. *Nat. Commun.* **14**, 769 (2023).
43. Draker, R. et al. A combination of H2A.Z and H4 acetylation recruits Brd2 to chromatin during transcriptional activation. *PLoS Genet.* **8**, e1003047 (2012).
44. Ding, Y. et al. Smarca5-mediated epigenetic programming facilitates fetal HSPC development in vertebrates. *Blood* **137**, 190–202 (2021).
45. Sun, G. et al. BAP18 facilitates CTCF-mediated chromatin accessible to regulate enhancer activity in breast cancer. *Cell Death Differ.* **30**, 1260–1278 (2023).
46. Pünzeler, S. et al. Multivalent binding of PWWP2A to H2A.Z regulates mitosis and neural crest differentiation. *EMBO J.* **36**, 2263–2279 (2017).
47. Sugeedha, J., Gautam, J. & Tyagi, S. SET1/MLL family of proteins: functions beyond histone methylation. *Epigenetics* **16**, 469–487 (2021).
48. Onrust-van Schoonhoven, A. et al. 3D chromatin reprogramming primes human memory T(H)2 cells for rapid recall and pathogenic dysfunction. *Sci. Immunol.* **8**, eadg3917 (2023).
49. Zhu, S. et al. Antigen exposure reshapes chromatin architecture in central memory CD8+ T cells and imprints enhanced recall capacity. *Proc. Natl Acad. Sci. USA* **120**, e2313476120 (2023).
50. Kreienbaum, C., Paasche, L. W. & Hake, S. B. H2A.Z's 'social' network: functional partners of an enigmatic histone variant. *Trends Biochem. Sci.* **47**, 909–920 (2022).
51. Hogquist, K. A. et al. T cell receptor antagonist peptides induce positive selection. *Cell* **76**, 17–27 (1994).
52. Faast, R. et al. Histone variant H2A.Z is required for early mammalian development. *Curr. Biol. CB* **11**, 1183–1187 (2001).
53. Langmead, B. & Salzberg, S. L. Fast gapped-read alignment with Bowtie 2. *Nat. Methods* **9**, 357–359 (2012).
54. Ramírez, F. et al. deepTools2: a next generation web server for deep-sequencing data analysis. *Nucleic Acids Res.* **44**, W160–W165 (2016).
55. Robinson, J. T. et al. Integrative genomics viewer. *Nat. Biotechnol.* **29**, 24–26 (2011).
56. Zhang, Y. et al. Model-based analysis of ChIP-Seq (MACS). *Genome Biol.* **9**, R137 (2008).
57. Liao, Y., Smyth, G. K. & Shi, W. featureCounts: an efficient general purpose program for assigning sequence reads to genomic features. *Bioinformatics* **30**, 923–930 (2014).
58. Brind'Amour, J. et al. An ultra-low-input native ChIP-seq protocol for genome-wide profiling of rare cell populations. *Nat. Commun.* **6**, 6033 (2015).
59. Li, H. et al. The sequence alignment/map format and SAMtools. *Bioinformatics* **25**, 2078–2079 (2009).
60. Yu, G., Wang, L. G. & He, Q. Y. ChIPseeker: an R/Bioconductor package for ChIP peak annotation, comparison and visualization. *Bioinformatics* **31**, 2382–2383 (2015).
61. Zhou, Y. et al. Metascape provides a biologist-oriented resource for the analysis of systems-level datasets. *Nat. Commun.* **10**, 1523 (2019).
62. Chen, T., Liu, Y. X. & Huang, L. ImageGP: An easy-to-use data visualization web server for scientific researchers. *iMeta* **1**, e5 (2022).


## Acknowledgements

We thank Xiaoyan Wang and Junying Jia for cell sorting, Institute of Biophysics, Chinese Academy of Sciences. We would like to thank the HPC-Service Station in Center for Biological Imaging, Institute of Biophysics, Chinese Academy of Sciences. This work was supported by the National Nature Science Foundation of China (82025015 and 32230038 to M.Z. and 82402042 to W.L.), National Key R&D Program of China (2019YFA0905903 to M.Z.), China Postdoctoral Science Foundation (2023M730796 to W.L.), and Postdoctoral Fellowship Program of CPSF (GZC20230600 to W.L.).

## Author contributions

W.L. and M.Z. designed the experiments. W.L., J.D., and M.Z. analyzed the data. W.L. conducted most experiments. Q.C., M.L., X.Y., and W.W. provided experimental guidance. Z.W. helped with RNA-seq analysis. S.Z. and X.C. provided mice. G.L. provided advice on project design. W.L. and M.Z. wrote the manuscript. M.Z. conceived and supervised the project.

## Competing interests

The authors declare that they have no conflicts of interest with the contents of this article.

## Additional information

**Supplementary information** The online version contains supplementary material available at https://doi.org/10.1038/s41467-025-62976-4.

**Correspondence** and requests for materials should be addressed to Mingzhao Zhu.

**Peer review information** *Nature Communications* thanks Eui-Cheol Shin, Hai-Hui Xue and the other anonymous reviewer(s) for their contribution to the peer review of this work. A peer review file is available.